

Extreme precipitation at Padang, Sumatra triggered by convectively coupled Kelvin waves

Natasha V. Senior^{1*} | Adrian J. Matthews^{2*} |
Benjamin G. M. Webber^{1*} | Stuart Webster³ |
Richard W. Jones³ | Donald S. Permana⁴ | Jaka A. I.
Paski⁴ | Riska Fadila⁵

¹Centre for Ocean and Atmospheric Sciences, School of Environmental Sciences and Climatic Research Unit, University of East Anglia, UK

²Centre for Ocean and Atmospheric Sciences, School of Environmental Sciences and School of Mathematics, University of East Anglia, UK

³Met Office, Exeter, UK

⁴Center for Research and Development, Indonesia Agency for Meteorology Climatology and Geophysics (BMKG), Jakarta 10610, DKI Jakarta, Indonesia

⁵West Sumatera Climatology Station, Indonesia Agency for Meteorology Climatology and Geophysics (BMKG), Padang Pariaman 25584, West Sumatera, Indonesia

Correspondence

N. Senior, School of Environmental Sciences, University of East Anglia, Norwich, NR4 7TJ, UK.
Email: n.senior@uea.ac.uk

Funding information

Newton Fund, UK Met Office through the FORSEA project, Grant/Award Number: DN373682; UK Natural Environment Research Council through the TerraMaris project Grant/Award Number: NE/R016704/1

* Equally contributing authors.

Convectively coupled Kelvin waves (CCKWs) are tropical weather systems that travel eastward along the equatorial waveguide and have been previously linked to 90% of flooding events in Sumatra, Indonesia. Here, the processes through which CCKWs influence convection to produce extreme precipitation are investigated, with a focus on Padang, a city on the west coast of Sumatra. Extreme precipitation days at Padang, defined as days when the daily total precipitation exceeds the 95th percentile, are found to be 59% more likely to occur given the presence of a CCKW. We find that CCKWs modulate the diurnal cycle to produce extreme precipitation. This is achieved through firstly providing low-level moisture and convergence that acts to couple the Kelvin wave to the convection. Secondly the CCKW acts to displace the convergence zone towards Padang such that it experiences rainfall that persists throughout the night and peaks the following day in the early evening. We examine case study of a CCKW that passed over Padang on 21st August 2017 bringing extreme precipitation that lead to flooding in the West Sumatra region, recording a maximum daily

accumulated rainfall of 137 mm. This case study showed remarkably similar characteristics in its propagation, structure and precipitation patterns to composite studies of CCKWs. The performance of a suite of convection-permitting configurations of the UK Met Office Unified Model (MetUM), embedded within a parameterised convection global model, in forecasting this CCKW is evaluated. In general all configurations of the model capture this event reasonably well. We find that extending the western boundary of the high-resolution model domain from 90°E to 65°E leads to a significantly improved forecast, as the CCKW development over the Indian Ocean is captured more accurately by the high-resolution nested model, compared with the lower-resolution global driving model.

KEYWORDS

convectively coupled equatorial wave, Kelvin wave, extreme precipitation, high impact weather, Sumatra, tropical waves, Indonesia

1 | INTRODUCTION

The Maritime Continent (MC) is one of the most convectively active regions on Earth, releasing energy that fuels global atmospheric circulation and influences weather and climate in remote regions (Ramage, 1968). At the heart of the MC lies Indonesia. Rainfall extremes are a major hazard experienced across the country's numerous islands. This can lead to floods and landslides (Hai et al., 2017; Hermawan et al., 2022; Purwaningsih et al., 2022), with devastating impacts on local populations. Convectively coupled Kelvin waves (CCKWs) are tropical weather systems that travel eastward along the equatorial waveguide, organising convection and forming an important mode of equatorial rainfall variability in the MC and influencing precipitation extremes (van der Linden et al., 2016; Ferrett et al., 2020; Lubis and Respati, 2021). A recent study revealed a strong link between CCKWs and high impact weather in the Indonesian island of Sumatra, with CCKWs being a factor in 90% of flood events in the region (Baranowski et al., 2020). In this study we will focus on the influence of CCKWs on rainfall extremes in Padang, a city that lies on the west coast of Sumatra (Figure 1). This is the capital city of the West Sumatra province and the most populous city on the west coast of Sumatra. High impact weather linked to extreme rainfall occurs often in the region, impacting livelihoods and posing a threat to life.

CCKWs are broadly similar to their dry theoretical counterparts (Wheeler and Kiladis, 1999), being nearly non-dispersive and propagating eastwards. CCKWs have been observed as tilting westward with height against the eastward direction of propagation independently of the background basic flow (Straub and Kiladis, 2003; Kiladis et al., 2009). Moist Kelvin waves also travel at considerably slower phase-speeds (Kiladis et al., 2009) of around 10–15 m s⁻¹ in the Indian Ocean (Roundy, 2008) and possess more complex propagation and growth mechanisms (Matthews, 2021) compared with dry Kelvin waves.

There is an increasing body of literature that links CCKWs (along with other equatorial waves) to precipitation extremes (e.g. van der Linden et al. (2016); Baranowski et al. (2020); Ferrett et al. (2020); Lubis and Respati (2021); Latos et al. (2021)). However, the mechanisms through which they organise convective systems to produce extreme precipitation are less well understood. Sumatra experiences a diurnal cycle of rainfall that is typical of islands in the MC, whereby convection peaks in the late afternoon over land (Qian, 2008), in the evening in coastal regions and in the early morning over the ocean (Yang and Slingo, 2001; Peatman et al., 2014). A land breeze front is created from the pressure difference that arises as land cools at a faster rate than the sea overnight. This land breeze propagates towards the coast in the evening and offshore overnight (Short et al., 2019; Bai et al., 2021). Recent studies found that convectively active phases of the Madden-Julian oscillation (MJO) can amplify the diurnal cycle of precipitation to produce extreme precipitation in regions of the MC, including western Sumatra (Ferrett et al., 2020; Da Silva and Matthews, 2021; Peatman et al., 2021). CCKWs are often embedded within the subscale anatomy of the MJO (Nakazawa, 1988; Kessler et al., 1995) and have their own interplays with the diurnal cycle of precipitation that have generally been found to increase the amplitude of diurnal cycle rainfall and alter timing of peak rainfall (Baranowski et al., 2016b; Vincent et al., 2016; Sakaeda et al., 2020). Baranowski et al. (2016b) found that CCKWs are more likely to traverse the MC when there is phase-locking between the convectively active phase of a CCKW and the diurnal cycle at Sumatra.

Global and regional climate models employing convective parameterisations have problems representing subscale processes such as deep convection, especially in the MC where complexities arise from the land-sea contrasts, coastlines and topography. Hence, the diurnal cycle of precipitation is poorly modeled (Love et al., 2011; Birch et al., 2015). The spectral power of OLR and precipitation associated with key modes of intraseasonal tropical variability, which include CCKWs, are underestimated in such global models (Menary et al., 2018; Williams et al., 2018; Dias et al., 2018; Roberts et al., 2019). There is a large improvement in representing the timing and peak rainfall of the diurnal cycle in convection permitting models, in addition to better representing extreme precipitation (Prein et al., 2015). Such convection-permitting models include the "regional-atmosphere-land" RAL1T (Bush et al., 2020) and RAL3 Met Office unified model (MetUM) configurations at 4.4 km and 8.8 km resolution, which will be used in this investigation.

We have identified Padang as an appropriate case study city for studying the link between CCKWs and high impact weather since this is one of the first equatorial cities in the path of a CCKW that traverses the Indian Ocean. Ferrett et al. (2020) identified the west coast of Sumatra as a region where there is high amplitude CCKW activity that coincides with significantly increased precipitation and Baranowski et al. (2016a) found that CCKWs arriving at Sumatra in phase with the diurnal cycle corresponded to higher precipitation amplitudes. Studying the processes through which CCKWs modulate the diurnal cycle of rainfall and influence rainfall extremes at Padang can provide a source of predictability leading to improved forecasts. Important for the convective processes at Padang is the Barisan mountain range (Peatman et al., 2021) which runs from the north west to the south east of the island whereby orographic uplift contributes to the occurrence of extreme rainfall at Padang. The orography also contributes to the regular occurrence of strong nocturnal rainfall in the seas offshore from Western Sumatra following a zone of cold surface outflow from the mountainous region (Wu et al., 2009). This is the reason precipitation occurs throughout the year at Padang. In this investigation we will focus on a case study during the JJA (June, July and August, Figure 1) where to the west of Sumatra there are south-easterlies and southerlies over the equatorial region.

In this paper the processes through which CCKWs trigger extreme precipitation at Padang, defined as days in which the total precipitation exceeds the 95th percentile (corresponding to 32 mm of daily rainfall), are investigated. Previous studies have established a link between CCKWs and precipitation extremes in Sumatra (Baranowski et al., 2016b; Ferrett et al., 2020; Baranowski et al., 2020). We study this link in greater depth through conducting a composite analysis of CCKWs and their role in triggering extreme precipitation in Padang and the west coast of Sumatra, to evaluate the mechanisms by which CCKWs alter the diurnal cycles of precipitation, wind and divergence. Through

comparing a database of CCKWs obtained during the first part of this study with extreme precipitation days at Padang, we identify a case study on 21st August 2017 which coincided with reports of flooding in the region (Akbar, 2017). This case study is used to explore in more detail how CCKWs interact with convective processes at Padang to produce extreme precipitation. Then the MetUM suite is evaluated for its performance in capturing these mechanisms during the 21st August 2017 extreme precipitation event.

2 | DATA AND METHODOLOGY

This study uses observations of precipitation rate from the Integrated Multi-satellite Retrievals for the Global precipitation measurement mission dataset (IMERG; Huffman et al. (2020)) and composites are compiled using precipitation from the Tropical Rainfall Measurement Mission 3B42 product (TRMM; Huffman et al. (2010)).

Wavenumber-frequency filtering to isolate CCKW signals was applied to equatorially averaged (2.5°S-2.5°N) TRMM precipitation data (Wheeler and Kiladis, 1999). A database of discrete CCKW events (eastward propagating trajectories) across the MC during the period 1st January 1998 to 31st December 2019 was then constructed by a methodology that followed local maxima in the CCKW-filtered precipitation data. Full details are in Matthews (2021) and Baranowski et al. (2016a). Wind and divergence data are taken from the ERA5 dataset (Hersbach et al., 2020). Daily accumulated rainfall data from 113 stations and relative humidity data from 12 hourly radiosonde ascents were supplied by the Indonesian Agency for Meteorology, Climatology and Geophysics (BMKG).

We evaluate the performance of a suite of MetUM South East Asia (SEA) convection permitting limited area models. These utilise a high-resolution atmospheric component that explicitly simulates convection. We analyse data from two 18-member convection permitting ensembles – one using the RAL1T science settings and the other using the RAL3 configuration. RAL1T utilises the Wilson-Ballard cloud microphysics scheme (Wilson and Ballard, 1999) and the prognostic cloud fraction and prognostic condensate scheme (PC2) (Wilson et al., 2008); the convection parameterisation scheme is switched off. For details of the parameterisations schemes used in RAL1T see Bush et al. (2020) which includes the full model description. In RAL3 the largest model upgrades compared with RAL1T are the introduction of the CASIM double-moment cloud microphysics scheme (Field et al., 2023) and the use of the bimodal large-scale cloud scheme (Van Weverberg et al., 2021). The RAL3 configuration is the latest version of the science configuration, whereas the RAL1T configuration produced the near-real-time forecasts. The purpose of comparing the two versions is to determine if and how the RAL3 configuration provides a better representation of the physical processes and forecasts the extreme rainfall event at longer lead times. Both these ensembles utilise the same domain spanning 115°N-15°S and 65°E-120°E. The ensembles are nested inside the Met Office Global and Regional Ensemble Prediction System – Global (MOGREPS-G) global ensemble from which they obtain their lateral boundary conditions during the forecasts (Walters et al., 2017). This global driving model parameterises convection and uses the GA6.1 science configuration. The MOGREPS-G ensemble is constructed with perturbations to the initial conditions and stochastic physics, SST and soil moisture (Inverarity et al., 2023). We also investigate a deterministic forecast: a 4.4 km resolution simulation using the RAL1T configuration, the domain spans 30°N-18°S and 90°E-154°E. This deterministic model was used to produce near-real-time forecasts for several countries in the region during the 21st August 2017 extreme rainfall CCKW event. Of particular interest in this study is the effect of extending the western boundary from 90°E in the near-real-time deterministic forecast to 65°E in our ensemble forecasts. All model runs presented in this paper are initialised at 00:00 UTC.

3 | INFLUENCE OF CCKWS ON EXTREME RAINFALL

Through examining the database of CCKWs across the MC, we find that they are a fairly common occurrence; between 1998–2019 there were 743 CCKWs crossing Padang corresponding to approximately 3 CCKWs per month. There is no preferred time of day nor time of year in which these CCKWs arrive at Padang, which is expected since CCKWs can form anywhere over the equatorial Indian Ocean and the spread of travel time to Padang results in a uniform distribution of arrival times there. There were 395 extreme precipitation days at Padang identified in TRMM precipitation data during this period. We find that 58 of the extreme precipitation days coincided with a CCKW crossing Padang on the (UTC) day and 173 extreme precipitation days occurred within ± 1 days of a CCKW crossing. If these events were probabilistically independent, we would expect around 37 extreme precipitation events to coincide with the passage of a CCKW and around 110 such events to occur within ± 1 day of a CCKW crossing. These correspond to a 59% and 60% increase in the chance of observing extreme rainfall on a given day at Padang if there is a CCKW crossing on the day and within ± 1 days respectively, compared to observing extreme precipitation alone. This corroborates findings in Baranowski et al. (2020) that CCKWs play an important role in influencing precipitation extremes in Sumatra.

We have seen that there is no significant difference between the chance of observing extreme precipitation on a given day if there is a CCKW crossing on that day or within ± 1 days. In order to understand how CCKWs influence local convection processes, we will focus only on those that cross Padang on the extreme precipitation day, defined as a day beginning at 00:00 UTC which correspond to a lag time $\tau = 0$.

The composite mean TRMM precipitation rate at lag $\tau = 6$ hours of the extreme precipitation days when a CCKW is present is shown in Figure 2 together with composite ERA5 surface winds. Here, the extreme events are composited with respect to 00:00 UTC (approximately 07:00 LST) on the day of extreme precipitation and τ is the lag from this time. This is the time of peak rainfall. At this point, the near-equatorial westerlies associated with the CCKW extend from the coast of Sumatra to beyond 90°E , between 5°S – 5°N . The Barisan mountains act to block the low-level westerly flow of the CCKW. This leads to the development of a northwesterly flow parallel to the mountain range. This could be thought of as a topographically trapped component of the CCKW travelling down the west coast. To the southwest of Sumatra there is a region of cyclonic vorticity which arises as the flow is diverted southwards along the barrier, generating vorticity downstream (Fine et al., 2016).

To determine the large-scale conditions associated with extreme precipitation at Padang, and then to determine if and how these conditions are modified by the presence of a CCKW, composites of TRMM precipitation, ERA5 zonal wind and divergence were analysed in Figure 3 for extreme precipitation days when no CCKW was crossing and separately for those when a CCKW was crossing on the UTC day.

The diurnal cycle of precipitation and low-level wind as described in e.g., Peatman et al. (2014) is well represented in the composite analysis, with the land breeze propagating towards the coast in the evening and offshore overnight. This can be seen in Figure 3a where the composite diurnal cycle of extreme precipitation days at Padang without a CCKW present is shown as well as the day before and the day after. Precipitation in Padang develops from around 16:00 LST ($\approx \tau = -15, 9, 33$ hours) each day and peaks around 21:00 LST ($\approx \tau = -10, 14, 38$ hours), with the precipitation envelope propagating offshore and remaining coherent to at least 95°E . The sea breeze (westerly anomalies, red contours), peaks at Padang around 12:00 LST ($\approx \tau = -19, 5, 29$ hours), then propagates offshore as the land breeze develops in the evening, with the weakest winds occurring in the early morning. The mornings are dry in all cases. On the extreme rainfall day beginning at 07:00 LST ($\tau = 0$ hours), the diurnal cycle is amplified in magnitude but follows the same pattern as other days. The composite 975 hPa wind divergence when there is no CCKW (Figure 3c) also follows a diurnal cycle, with convergent winds leading the convection and propagating offshore with the variation in the land and sea breezes, whilst dry periods in the local mornings are led by divergence. Hence, extreme precipitation days in

the absence of a CCKW behave as amplified versions of the standard diurnal cycle of precipitation and circulation.

However, when a CCKW is present on an extreme precipitation day, the diurnal cycle of precipitation is altered (Figure 3b). A larger eastward-propagating envelope of precipitation associated with the CCKW modulates the smaller-scale westward propagating envelopes of the diurnal cycle precipitation. On the day before the extreme precipitation day, the convection propagating offshore is amplified by the large-scale convergence and ascent associated with the CCKW. We have noted that generally CCKWs cross Padang at any time of day however we see here that the convective phases of CCKWs associated with extreme precipitation appear to coincide with periods of active diurnal cycle convection. As described in (Baranowski et al., 2016b), CCKWs arriving in phase with the diurnal cycle in this way, are likely to be enhanced by the convective processes already present due to convergence ahead of the land breeze front; here we see the converse is also true, with the CCKWs associated with extreme precipitation enhancing the diurnal rainfall peak. At Padang the rainfall persists through the night following the evening spike in precipitation associated with the diurnal cycle of the previous day. By lag $\tau = 0$ hours, the westerlies and convection from the incoming CCKW have converged with the easterlies and the diurnal convection cycle from the evening land breeze the day before. The composite mean rainfall at Padang on the extreme precipitation day persists overnight and steadily rises from the morning (around $\tau = 3$ hours) to a peak in the early evening at $\tau = 12$ hours, in contrast to the case where there is no CCKW, for which precipitation is at a minimum around $\tau = 3$ hours and increases from around $\tau = 9$ hours to a peak in the evening ($\tau = 14$ hours). The offshore propagation of the convective envelope associated with the diurnal cycle is suppressed later on in the extreme rainfall day as the CCKW propagates past Padang. This can be understood by examining the composite 975 hPa wind divergence (Figure 3d). A large westward propagating region of convergence precedes the convection associated with the CCKW and at the western edge of the convective envelope there is a region of divergence (Straub and Kiladis, 2003). Hence we find that the convergence and divergence of the CCKW modulate the diurnal cycle of rainfall to produce an extended period of heavy rain with an earlier peak.

To ensure that the trends established in the composite analysis (given by Figure 3) are not biased by outliers, we calculate the 24 hour running-mean TRMM precipitation rate at Padang of all 58 extreme precipitation days that coincided with a CCKW crossing Padang (Figure 4) and examine their distribution. The median 24 hour running-mean precipitation rate peaks between $\tau = 3 - 15$ hours which is similar to that of the mean precipitation rate that peaks between $\tau = 6 - 18$ hours. The distribution is not symmetric about $\tau = 12$ hours; the median 24 hour running-mean precipitation rate at $\tau = -12$ hours (0.8 mm hour^{-1}) is significant compared to $\tau = 36$ hours where the precipitation rate falls to zero. Furthermore the events are not uniformly distributed about the median between $\tau = -12 - 0$ hours, there are a large spread of events in the upper-quartile suggesting a tendency for extreme precipitation events to occur during this time period. This is consistent with our composite analysis where we found that rainfall at Padang begins in the evening and persists overnight as the convergence line draws closer to Padang as the CCKW approaches (Figure 3d). Conversely, we found that there was a suppression of convective processes when the divergent phase of the CCKW crosses which is consistent with the median 24 hour running-mean precipitation rate falling to zero at $\tau = 36$ hours.

4 | 21ST AUGUST 2017 CCKW CASE STUDY

In this section, a case study of a CCKW associated with extreme precipitation over Padang is chosen, to examine processes associated with an individual event, and to assess the ability of the Met Office convection permitting forecast model to accurately capture the timing and relevant physical processes of the interaction between the CCKW and extreme precipitation. On 21st August 2017 a CCKW passed over Padang that corresponded to one of the extreme

precipitation days identified. This particular event was chosen as it was an isolated CCKW that did not coincide with an active MJO phase and showed little other convective activity that was not related to the CCKW.

4.1 | Observations

The CCKW initiated in the Indian Ocean on 19th August 2017 around 03:00 UTC and travelled eastward at around 10° longitude per day which can be seen in the Hovmöller of the IMERG precipitation rate and ERA5 10 m surface zonal wind contours over this period (Figure 5a). On 21st August 2017, a band of heavy rainfall passed over Padang and traversed Sumatra over the course of the day, coinciding with the CCKW trajectory. The precipitation on the days prior to the CCKW passing over Padang showed little convective activity onshore and offshore. The climatology during JJA is predominantly easterlies (Figure 1). The trajectory of the CCKW, calculated from the precipitation signal, is preceded by strong easterlies and followed by strong westerlies giving rise to regions of convergence that are convectively active (Figure 5a). Convective activity appears to have been triggered just offshore from Padang through coupling between the land breeze and the westerly winds of the CCKW. This deviates slightly from the composite analysis, which shows that the diurnal cycle of convection is amplified rather than triggered by the CCKW during extreme precipitation events associated with a CCKW. On the day of extreme precipitation, offshore convection steadily approached Padang overnight and rose to a peak in Padang at 05:00 UTC (12:00 LST, Figure 5b). We also find that stations in the vicinity of Padang recorded an average daily accumulated rainfall of 32.46 mm from 00:00-23:59 UTC on 21st August 2017 which aligns well with that of IMERG data which showed 36.88 mm (Figure 5b).

The IMERG precipitation and surface wind anomalies at different times are shown in Figure 6 for this case study. At 12:00 UTC on 20th August 2017 (19:00 LST, Figure 6a), the CCKW can be seen approaching Padang as a broad region of near-equatorial westerly wind anomalies. There is also some convection offshore at this time. At 00:00 UTC on 21st August 2017 (07:00 LST, Figure 6b) the CCKW made landfall at Padang, bringing heavy precipitation at Padang and over the ocean to the west, with peak precipitation in Padang at 05:00 UTC (14:00 LST, Figure 6c). Wind vectors started to orient parallel to the coast as a component of the CCKW became topographically trapped by the Barisan mountain range and winds began to travel southeastwards. This figure shows striking similarity to the composite precipitation and surface wind anomalies during extreme rainfall days associated with CCKWs around this time (Figure 2). As we have seen in the composite analysis, the convergence provided by the CCKW is a key mechanism that enhances the rainfall intensity at Padang which is evident through inspection of the wind field. At 16:00 UTC ($\tau = 16$ hours, Figure 6d) Padang was anomalously dry as the divergence following the CCKW (evident in the diverging wind vectors around Padang) acted to suppress the convective processes, while anomalous westerly wind vectors parallel to the equator can be seen to the east of Sumatra as the CCKW travelled towards Borneo.

The CCKW increased the low-level moisture through advection of moist air from the ocean. This can be understood by examining the anomalous divergence of the ERA5 vertically integrated water vapour transport (IVT) (Figure 6a) at the time when there was maximum precipitation at Padang at 05:00 UTC ($\tau = 5$). A band of moisture convergence is aligned along the western coastline of Sumatra at this time in the vicinity of Padang that coincides with a region of increased precipitation (Figure 6c). The divergence of IVT was approximately $-1 \times 10^{-3} \text{ kg m}^{-2} \text{ s}^{-1}$ which corresponds to a precipitation rate of approximately 100 mm day^{-1} . The eastward direction of the mass flux is similar to the direction of the surface winds at this time, which then turn southeastward as the CCKW approached the Barisan mountain range. Thus orographic uplift likely contributed to the moisture convergence in this region. The Sumatra vortex that was positioned in the Indian Ocean at around 93°E also possessed a region of strong moisture convergence that roughly coincided with an increased precipitation rate.

Further evidence of the impact of the CCKW on humidity is gained from the radiosonde profiles from Padang

(Figure 6b). As the CCKW approaches Padang, the low-level (1000-800 hPa) relative humidity increases to over 90% early on 21st August, coinciding with the peak in rainfall. The relative humidity then rapidly decreases after this time, to only 60% on 22nd August, once the CCKW has passed through. Additionally, a rapid increase in relative humidity is observed at middle levels (600-400 hPa) during the passage of the CCKW, presumably due to detrainment of moisture by convection in the active part of the CCKW.

The vertical structure of the 21st August 2017 CCKW is similar to that of composites of CCKWs described in, e.g., Kiladis et al. (2009) (Figure 8). This is an interleaving pattern of westward tilting (i.e., against the direction of eastward propagation) easterly and westerly wind anomalies that extend up to the tropopause. The longitude axis may effectively be replaced by an inverted lag time axis as shown in Figure 8a of Kiladis et al. (2009) as this whole structure moves eastward with time. At Padang itself, the surface winds switch from easterly to westerly anomalies at 00:00 UTC ($\tau = 0$). This marks the convergent phase of the CCKW which is associated with deep convection. This can be seen in Figure 6b at 00:00 UTC ($\tau = 0$) when the heavy rainfall begins.

4.2 | Representation in MetUM forecasts

8.8 km resolution convection-permitting MetUM regional ensemble simulations have been run for this case study period. The simulations have been performed with the convection parameterisation scheme switched off and using two different RAL physics configurations, RAL1T and RAL3. 18 ensemble members are run for each forecast initialisation time. The key updates to the atmospheric model in RAL3 are the introduction of both the CASIM double moment cloud microphysics scheme and the bi-modal cloud scheme. During the evaluation of RAL3 the CASIM microphysics was shown to improve the aerosol-cloud interactions and lead to less intense precipitation within the centre of convective cells, while increasing the amount of light-stratiform rain around precipitating cells. We examine ensemble mean forecasts at 8.8 km resolution at an early (17th August 2017) and late (19th August 2017) initialisation time for each configuration (Figure 9). The western boundary is extended beyond the near-real-time forecast domain for this region from 90°E to 65°E in order to capture the CCKW initiation in the Indian Ocean on 19th August 2017 at approximately 03:00 UTC (Figure 5).

First, we examine the ensemble of RAL1T 8.8 km forecasts initialised on 17th August 2017 (Figure 9a), 2 days before the CCKW was triggered. The ensemble mean successfully predicts the initiation of a CCKW, producing a band of eastward propagating precipitation generally following the same slope as the observed CCKW trajectory. However there is variability between the individual ensemble members.

A majority of the RAL1T ensemble members, in addition to forecasting a precipitation trajectory that aligns with that of the observed, forecast a convective system that propagates at approximately half the speed of the CCKW. One of these ensemble members is shown in Figure 10, where pulses of precipitation can be seen tightly coupled to slowly propagating westerlies emanating from the region in which this convective signal initiates in the Indian Ocean, around 85°E. These features have also been observed in Weather Research and Forecasting (WRF) aquachannel simulations, discussed in (Blanco et al., 2016) as an interaction between the CCKW and slower moving Super Cloud Clusters which go through many life cycles of growth and decay within the CCKW envelope, acting to slow the CCKW trajectory. As a result, there is variation between individual ensemble members comprising Figure 9a with several members even forecasting the arrival of these propagating features a day late, resulting in a spike of forecast precipitation in Padang at 15:00 UTC on 22nd of August (Figure 9b). However, other ensemble members do correctly predict the trajectory of the CCKW, which is evident in Figure 9a as the climatological easterlies weaken in the region of the observed trajectory of the CCKW coinciding with heavy rainfall, consistent with the presence of a CCKW. These correctly forecast heavy rainfall at Padang on the 21st of August.

The ensemble mean RAL1T forecast predicts overly persistent rainfall along the CCKW trajectory; however, the simulated westerly anomalies are weaker (Figure 9a) when compared with IMERG and ERA5 data (Figure 5). This suggests that the coupling between the winds and the convection is too weak in the RAL1T configuration and that the model overestimates the convective response of the wave. In the days preceding the passage of the CCKW, the diurnal cycle is strong in the RAL1T ensemble (Figure 9a), with envelopes of high amplitude precipitation propagating offshore following the easterly wind anomalies of the land breeze. This was not present in the IMERG data where conditions were relatively dry. In the vicinity of Padang (Figure 9b), although there is variability between ensemble members evident in the large interquartile range, the ensemble average predicts well the amplitude, timing and duration of rainfall as the CCKW passes over Padang on 21st August 2017.

The ensemble of RAL1T 8.8 km forecasts initialised later, on 19th August 2017, contains the propagating CCKW within its initial conditions (Figure 9c). As expected given the short lead time there is a marked improvement in forecasting the event compared to the forecast initialised on 17th August 2017 (Figure 9a). There are pulses of precipitation that follow the observed trajectory and occur at similar times to the observed, with suppressed convection in between, until the CCKW approaches the west coast of Sumatra and interacts with diurnal cycle on the 20th of August. In the observations, we found that the diurnal cycle of convection was greatly influenced and amplified by the incoming CCKW (Figure 5). In contrast, the RAL1T ensemble shows a substantial amount of evening rainfall associated with the diurnal cycle that has a similar size peak to the morning rainfall associated with the CCKW. The erroneous spike in precipitation at 15:00 UTC on 22nd August 2017 remains in this forecast, albeit weaker, associated with the slower propagating convective features that were seen in the forecast initialised on 17th August 2017 (Figure 9a), but not observed in the IMERG data (Figure 5). Fewer ensemble members in the forecast initialised on 19th August (Figure 9c) demonstrated these features when compared to ensemble members comprising the forecast initialised 17th August (Figure 9a), which is why the slow propagating features are less prominent in this forecast and the peak of rainfall on 22nd August at Padang (Figure 9d) has a lower amplitude.

The effect of the location of the western boundary of the high-resolution model on the CCKW forecast was then investigated. In the ensemble runs described above, the western boundary was set at 65°E. Hence, the high-resolution model encompassed the genesis location of this particular CCKW, at 78°E. Here, we investigate the same CCKW but in the near-real-time version of the model, which has the western boundary of the high-resolution model set at 90°E. Hence, the genesis of this particular CCKW would be simulated by the lower resolution, parameterised convection global driving model and propagated into the higher resolution model through the western boundary conditions. In Figure 11 we show the Hovmöller diagram of the 4.4 km deterministic SEA RAL1T MetUM forecast. The initialisation times compared in this figure are a day apart.

Examining the forecast initialised on 19th August 2017 (Figure 11a), there is little evidence of a CCKW. Although there is some eastward propagation of convection that interacts with a westward propagating region of convection associated with the diurnal cycle on 19th August 2017 and Padang experiences rainfall overnight (Figure 11b), these do not align with the observed trajectory of the CCKW, which propagates at a faster speed. Furthermore, for this particular case study, the observed amplitude of rainfall was low overnight, underlining the poor representation of the rainfall in this forecast.

There is a significant improvement when the forecast is initialised on 20th August 2017 (Figure 11c), with an eastward propagating convective system that aligns with the observed CCKW trajectory. The timing, amplitude and trajectory of the precipitation is captured realistically by the model, with strong offshore precipitation that propagates over Padang and towards Borneo by the end of the day. The peak forecasted precipitation occurs around 09:00 UTC on 21st August 2017 (Figure 11d) which is slightly later than the peak rainfall observed in the IMERG data (Figure 6b) at 05:00 UTC. The precipitation associated with the diurnal cycle on 20th August 2017, the day before the extreme

precipitation day, is amplified as anomalous easterlies coincide with the anomalous westerlies from the approaching CCKW. Although this eastward propagation offshore of the convective system associated with the diurnal cycle was not as strong in the observations for this case study, it is evident in the forecast that there is a convective system associated with a coupling between the diurnal zonal wind cycle and the incoming CCKW. The signal also appears in the total zonal wind field, seen as contours of westerlies over Padang on Figure 5, which is represented faithfully in this forecast (Figure 11c).

This marked improvement between the two RAL1T deterministic forecasts with western boundary at 90° E (Figure 11) can be attributed the CCKW signal being more or less present within the model's initial conditions for the forecast initialised on 20th August 2017 (Figure 11c). This is because it is forced at the western boundary by the global driving model with a strong westerly wind signal associated with the CCKW. In contrast, the CCKW signal was at approximately 80° E in the global driving model for the forecast initialised on 19th August 2017 (Figure 11a). Since the global model poorly represents the propagation of convectively coupled equatorial waves (Dias et al., 2018; Roberts et al., 2019), the signal in the wind field as well as the precipitation field was spun down by the time the wave was observed to approach the western boundary at 90° E.

Overall, we find that shifting the western boundary from 90° to 65° , such that the convection-permitting region of the forecast is extended, results in skilful lead times being significantly increased, from 1 day to at least 4 days. This is because allowing for explicit convection over a longer range, results in the genesis, coupling between the CCKW and wind fields and the trajectory of the CCKW being well simulated. Whereas, models with smaller domain extents are more reliant on the boundary forcing by the global model, which suppresses this long-range signal at longer lead times. This results in an inaccurate representation of the CCKW in the boundary forcing.

The advantage, however, of having the western boundary at 90° E is a more accurate forecast at short lead times of 1 day. The RAL1T deterministic forecast with western boundary at 90° E (Figure 11c) best captured the coupling between the CCKW and the diurnal cycle, the amplitude and timing of rainfall at Padang and the wind field associated with the observed CCKW trajectory of all the forecasts examined. This forecast outperformed the forecasts initialised on the extended western boundary out to 65° E at this lead time. This is because the boundary forcing at 90° anchors the CCKW at the observed spatial and temporal location, compared to the ensembles with western boundary at 65° E where the forecasted trajectories could vary due to the simulated location of CCKW initiation and propagation speed.

4.3 | Ensemble forecast performance at Padang

We have seen that forecast performance improves as the lead time shortens, with more realistic simulated CCKW propagation and associated rainfall patterns. We now study this further and consider if this leads to improvements in the simulated rainfall rates at Padang. We do so by examining ensemble mean precipitation rates and their spread at four different initialisation times for both RAL1T and RAL3 configurations at 8.8 km resolution on the extended domain (Figure 12). An ensemble of RAL1T configurations at 4.4 km resolution was also run and compared to those at 8.8 km. It was found that there was no qualitative difference.

The forecasted RAL1T ensemble mean precipitation rate at Padang, at the time the CCKW crosses, improves with later initialisation times (Figure 12a-d). However, there is a consistent overestimation of the rainfall amplitude on the days prior to the passage of the CCKW on 21st August 2017 in this configuration. There is a small peak of diurnal rainfall in the observations on 20th August 2017 that is greatly exaggerated in the ensemble mean across all initialisation times, although the timing of the onset of diurnal precipitation improves with later initialisation times. As demonstrated in the composite analysis (Figure 3), there is often an increase in diurnal rainfall amplitude ahead of the arrival of the CCKW, which may be what the model is capturing, though in this particular case study this interaction

was relatively weak. The simulated rainfall at Padang on the extreme precipitation day associated with the passage of the CCKW (21st August 2017), peaks with a comparable amplitude to the observed; however, the timing of the peak is later than the observations at 09:00 UTC compared to 05:00 UTC in the observations. The simulated rainfall associated with the CCKW passage does fall off at a similar rate to the observations (Figure 12a-d), as the divergent phase of the CCKW begins to suppress the offshore propagation.

The RAL1T forecasts do not clearly identify 21st August 2017 as an extreme precipitation day relative to the neighbouring days. This is evident in Figure 12a (initialised on 17th August 2017) where there is significant simulated convection between 17th-18th August 2017 that has comparable duration and amplitude to that of, 21st August 2017. As noted previously, on 22nd August 2017 at 12:00 UTC (Figure 12, there is a peak of rainfall that is not present in the observations. This corresponds to the slow-propagating CCKW-like convective features seen in Figure 10 that travel around half the speed of the CCKW simulating the arrival of the CCKW a day later. This peak reduces in amplitude with later initialisation times.

In the RAL3 configuration, there is an improvement in the timing and simulation of diurnal rainfall intensity at Padang when compared to the RAL1T configuration (Figure 12e-h), but, similarly to RAL1T, this package also demonstrates only small improvements as the lead time shortens. The amplitude of rainfall on the extreme precipitation day is underestimated, however the forecasts robustly identify 21st August 2017 as a day with relatively high precipitation even at earlier lead times. Furthermore, the simulated diurnal rainfall peak on 20th August 2017 occurs at the observed time (18:00 UTC). On 21st August 2017, the day the CCKW passes over the Padang, the timing of the peak of rainfall is also later than observed, arriving at 09:00 UTC (Figure 12e-h), a similar delay to RAL1T. There remains an erroneous peak of rainfall on 22th August 2017; however, relative to RAL1T, there is a greater spread between ensemble members that simulate this as reflected in the wider interquartile range, with fewer RAL3 ensemble members simulating the slow-propagating eastward moving convective features that result in the CCKW arriving a day late at Padang.

Both model configurations simulate a robust precipitation rate at Padang that varies little between lead times, even at lead times in which the CCKW has not yet initiated (before 19th August 2017). This is a testament to the performance of the models in accurately simulating the initiation of the CCKW in the Indian Ocean such that the precipitation rate signal is robust at longer (Figure 12d and f) and shorter (Figure 12b and f) lead times. However, the timing of the peak of the precipitation is consistently late across all lead times in the RAL3 and RAL1T ensembles suggesting some other model bias. This is discussed below.

We further investigate how the RAL1T and RAL3 configurations simulate peak rainfall time and amplitude by examining the 24 hour running-mean precipitation rate of the ensembles initiated on 19th August 2017 (Figure 13). A running time mean is chosen to smooth fluctuations in rainfall intensity that may mask an underlying trend and the 24 hour window is chosen as this is the interval over which we define an extreme precipitation day.

The observed 24 hour running mean precipitation rate peaks at 03:00 UTC and almost plateaus until 12:00 UTC after which the running-mean rainfall rate falls. The amplitude of the median 24 hour running-mean peak rainfall rate of the RAL1T configuration itself (Figure 13a) is comparable to the observed however, differently from that of the observed, it peaks twice, first on 20th August 2017 at 21:00 UTC and second on 21st August 2017 at 06:00 UTC. The upper quartile of ensemble members with more extreme precipitation rates are skewed towards the earlier rainfall peak. The first peak is influenced by the large diurnal cycle peak that many of the RAL1T ensemble members exhibit (Figure 12c) whilst the second is associated with the simulated CCKW convective envelope. However, there was only a small diurnal rainfall peak in the vicinity of Padang during this particular event (Figure 5; this period of rainfall is mostly driven by the CCKW. The amplitude of the median 24 hour running-mean peak rainfall rate of the RAL1T configuration itself is comparable to the observed. However, as we have noted previously, the RAL1T configuration

overestimates rainfall, such that the simulated rainfall is less extreme relative to other days than observed, which reduces the predictive value.

The median 24 hour running-mean precipitation rate of the RAL3 ensembles peaks once on 21st August 2017 03:00 UTC (Figure 13b), at the same time as the observed peak. This suggests that ensemble members in the RAL3 configuration are better able to capture the timing of the arrival of the CCKW and its interaction with diurnal cycle. The amplitude of this peak is low compared to that of the observed and only 2 ensemble members are able to simulate a 24 hour running-mean precipitation rate that is comparable to the observed.

5 | DISCUSSION

5.1 | Key processes

A key process identified in our composite studies, through which CCKWs may trigger extreme rainfall at Padang, is a coupling between the convection associated with the CCKW with that of the diurnal cycle. The CCKW provides additional convergence and moisture to the land breeze front, amplifying the convection and increasing the chance of extreme rainfall. This process begins the evening prior to the extreme rainfall day at Padang as the diurnal cycle of precipitation propagates offshore and interacts with the CCKW. The CCKW then draws closer to Padang overnight, the convection is established and is sustained by the CCKW and rainfall persists overnight, rather than being suppressed by the divergence of the diurnal cycle as morning approaches. This process was reflected to some degree in the 21st August 2017 case study in which convection was triggered offshore by the incoming CCKW which lead to rainfall at Padang increasing at 00:00 UTC to a peak at 05:00 UTC. Later on in the day, the rainfall rate diminishes and Padang becomes anomalously dry as the divergent phase of the CCKW passes over and inhibits convection.

5.2 | Forecast domain

A comparison of forecasts in different domains suggests that having a larger domain size of the convection-permitting forecast model was crucial for accurately predicting the 21st August 2017 CCKW that brought extreme rainfall to Padang.

The SEA RAL1T 4.4 km deterministic forecast with the western boundary at 90°E did not faithfully represent the observed trajectory of the CCKW at earlier lead times (Figure 11a), capturing neither the CCKW interaction with the diurnal cycle nor the peak precipitation amplitude. However, the performance of this forecast significantly improved when the lead time was shortened (Figure 11c). This was because the global driving model, in which the deterministic forecast is nested, poorly represented the CCKW trajectory and its convection since convection is parameterised in this model (Love et al., 2011; Birch et al., 2015). Only when the CCKW was present within the initial conditions of the convection-permitting forecast, at a short 1-day lead time, did the forecast trajectory, total wind field and convection of the CCKW resemble the observed. The ensembles over the extended domain, with western boundaries at 65°E, performed well at longer lead times, benefiting from being able to capture the initiation and evolution of the CCKW. Though the exact trajectory of the CCKW varied between ensemble members, all ensemble members demonstrated some evidence of a CCKW, with eastward propagating convection coinciding with converging zonal winds (Figure 9).

5.3 | Model physics configurations

We have compared two MetUM regional physics configurations RAL1T and the more recently developed RAL3. Both of these consistently predicted a later arrival of the CCKW at 09:00 UTC compared to 05:00 UTC in the observations at all lead times. One possible explanation for this could be a poor representation of the interaction between the CCKW and the diurnal cycle. Also the ensemble averages (Figure 9) both demonstrate strong diurnal cycles of precipitation, particularly in the RAL1T configuration, which may act to overwhelm the CCKW that is comparatively stronger in observations (Figure 5). In the RAL3 configurations, the westerlies associated with the sea breezes are particularly pronounced. This issue could also in part be due to the CCKW arrival time varying between ensemble members, with many ensemble members demonstrating slow-propagating convective features, such that the signal from the CCKW is not well represented in the mean. When there are fewer of these slow-propagating signals, in both RAL1T and RAL3, the interaction between the diurnal cycle and the CCKW is well simulated.

The deterministic RAL1T configurations with western boundaries at 90°E, initialised at early times in which the CCKW lies outside the boundary, poorly represented the CCKW because of the poor representation of equatorial waves in the global model that forces the boundary (Dias et al., 2018; Roberts et al., 2019). One advantage of the RAL1T deterministic forecast with the domain boundary at 90°E was that the CCKW was initialised at the correct location on 20st August 2017 (Figure 11b) which eliminated issues with slow propagation of the CCKW seen in some of the extended-domain forecasts. This could reduce the spread of CCKW arrival times in ensembles. However, since CCKWs travel at around 10° per day, this would only provide an accurate forecast at a lead time of 1 day which is relatively short for predicting a high impact weather event. Given the importance of CCKWs for extreme rainfall an ensemble of forecasts on an extended domain may be more useful for assessing risks associated with the presence of a CCKW even if the timing of arrival of the CCKW is not accurate.

In all cases the RAL1T configurations overestimated the mean rainfall rate throughout the forecast so although the extreme rainfall due to the CCKW had similar magnitude to the observations, the observed relative peak in daily rainfall was not captured. Furthermore, in the RAL1T configuration, the time of the peak ensemble median 24 hourly mean precipitation rate was early compared to that of the observed, whereas that of the RAL3 configuration matched the observed. It is possible that within the RAL1T simulations the daily precipitation rate on 21st August 2017 would not exceed the 95th percentile and be considered an extreme precipitation day. The CASIM microphysics scheme introduced in RAL3 is known to reduce convective rainfall intensity, this was evident in the RAL3 ensembles, which more faithfully represent the observed precipitation amplitude in general and provided a starker contrast between the extreme precipitation day and others.

Ensembles of SEA RAL1T and RAL3 8.8km forecasts also benefited from averaging over multiple realisations. Some simulated the precipitation peak at Padang at the correct time whilst others simulated it a day late. This could be attributed to slowly propagating features that were tightly coupled to the convection as described in Blanco et al. (2016). This was evident in many of the ensemble members, particularly in the RAL1T configurations in which the convection is stronger. At later initialisation times, the forecast time of peak precipitation improved in the ensembles but particularly for the RAL3 configuration, in which these slowly propagating features were suppressed compared to the RAL1T configuration.

5.4 | Future Work

There are several avenues of future exploration that could improve our understanding of CCKWs and how they modulate rainfall extremes. Sumatra experiences rain year-round due to the presence of the Barisan mountains however

there is a sharp contrast between seasons in wind direction. It would be useful to understand how these processes are altered by seasonal differences through comparing case studies in the boreal summer and winter. Our composite studies included all CCKWs without distinguishing between MJO phases; further work could investigate CCKW interactions with the diurnal cycle are modulated by the MJO and how the MetUM configuration represents such multiscale interactions. In the composite study and the case study, a region of vorticity offshore from Padang coincided with the arrival of the CCKWs which we identified as the Sumatra vortices (Fine et al., 2016; Latos et al., 2021). How the Sumatra vortices contribute to the propagation and convective properties of the CCKWs and if they play a role in enhancing onshore precipitation, remains an open question.

6 | CONCLUSION

Through examining a database of CCKWs that have crossed Padang in the period 1998-2020, we have found that there is a 59% increase in chance of observing extreme precipitation at Padang given the presence of a CCKW compared to extreme rainfall alone. We have found that CCKWs modulate the convective processes associated with the diurnal cycle to produce extreme rainfall through studying composites of lagged precipitation, wind and divergence for days with and without a CCKW present (Figure 3). The convection and low-level moisture associated with the convergent phase of the CCKW becomes coupled to the diurnal cycle. This results in the presence of overnight rainfall at Padang as the CCKW displaces the convergence zone towards Padang and rainfall steadily increases through the morning and peaks in the early evening at $\tau = 12$ hours. Then, as the CCKW traverses Sumatra, evening rainfall at Padang is suppressed following the divergent phase of the CCKW.

A case study of a CCKW linked to extreme rainfall at Padang on 21st August 2017 bore striking resemblance to those described in the literature (e.g., Kiladis et al. 2009) with anomalous easterlies switching to anomalous westerlies at the onset of convection and tilting westward with height. This case study also demonstrated many of the mechanisms identified in our composite studies, with rainfall rates increasing overnight to a peak the following day and suppression of the diurnal cycle later in the day leading to dry evening conditions (Figure 6d).

We have found a variety of factors that influence a model's performance in capturing the CCKW. Ensembles of convection-permitting RAL1T and RAL3 8.8km forecasts (Figure 9), running on an extended longitude domain (western boundary at 65°E) compared to the standard SEA domain (western boundary at 90°E), capture the propagation of the CCKW and its interaction with the diurnal cycle well even in the early forecasts that are initialised before the formation of the CCKW in the Indian Ocean. There is a marked improvement in the forecast performance, particularly in the propagation of the CCKW and its associated convection, when the forecast initialisation times are closer to the extreme event. However, the timing of the precipitation peak associated with the CCKW at Padang varies between ensemble members, with many predicting a slower propagation of the CCKW trajectory than the observed, possibly due to interactions with Super Cloud Clusters.

The CCKW was poorly represented in early initialisation times of the MetUM SEA RAL1T 4.4 km deterministic forecast when the CCKW is outside the domain boundary (90°E). The trajectory and convection properties of the CCKW was poorly represented by the global driving model, in which this model is nested such that boundary forcing did not influence greatly the performance. There was a significant improvement however when the CCKW is present within the initial conditions. Whilst this arguably provides the best representation among the forecasts examined, it is more useful for forecasters to be aware of the potential impact of a CCKW using an ensemble of forecasts on a domain that captures the CCKW's full evolution, even if its exact trajectory and day of impact is uncertain, than having an accurate forecast at short lead time. This demonstrates a key benefit of extended-domain convection-permitting

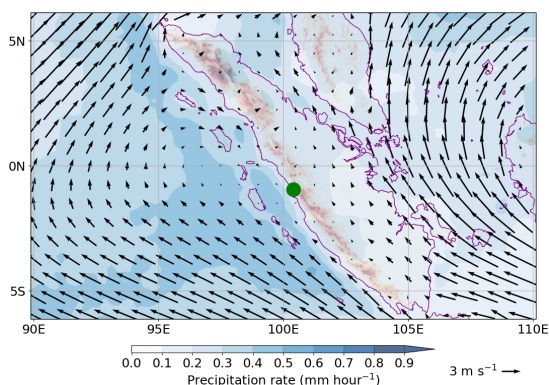


FIGURE 1 Climatological mean TRMM precipitation rate and ERA5 vector surface winds for JJA 1998–2019. Precipitation rate is colour shaded in blue (interval 0.1 mm hour^{-1}). The standard wind vector is 3 m s^{-1} . Topography is shown in both panels by the red colour shading (interval 250 m). The location of Padang is shown by the green filled circle.

models in improving forecasts of propagating weather systems at longer lead times.

acknowledgements

The IMERG precipitation data were supplied by the National Aeronautics and Space Administration through their web site at gpm.nasa.gov. The ERA5 data were provided by the Copernicus data centre at cds.climate.copernicus.eu. NVS, AJM and BGMW were supported through the Forecasting in Southeast Asia (FORSEA) project, funded by the Newton Fund through the Weather and Climate Science for Service Partnership (WCSSP) of the UK Met Office (award DN373682), and AJM was supported through the TerraMaris project, funded by the Natural Environment Research Council (award NE/R016704/1). We thank the anonymous reviewers for their helpful comments and suggestions for improving this manuscript.

references

- R. Akbar. Diguyur Hujan dari Pagi, Ratusan Rumah di Padang Pariaman Terendam Banjir 1,5 Meter. *Okezone*, 2017. URL <https://news.okezone.com/read/2017/08/21/340/1759869/diguyur-hujan-dari-pagi-ratusan-rumah-di-padang-pariaman-terendam-banjir-1-5-meter>.
- H. Bai, G. Deranadyan, C. Schumacher, A. Funk, C. Epifanio, A. Ali, Endarwin, F. Radjab, R. Adriyanto, N. Nurhayati, Y. Nugraha, and A. Fauziah. Formation of Nocturnal Offshore Rainfall near the West Coast of Sumatra: Land Breeze or Gravity Wave? *Monthly Weather Review*, 149(3):715 – 731, 2021. doi: 10.1175/MWR-D-20-0179.1. URL <https://journals.ametsoc.org/view/journals/mwre/149/3/MWR-D-20-0179.1.xml>.
- D. B. Baranowski, M. K. Flatau, P. J. Flatau, and A. J. Matthews. Impact of atmospheric convectively coupled equatorial Kelvin waves on upper ocean variability. *Journal of Geophysical Research: Atmospheres*, 121(5):2045–2059, 2016a. doi: <https://doi.org/10.1002/2015JD024150>. URL <https://agupubs.onlinelibrary.wiley.com/doi/abs/10.1002/2015JD024150>.
- D. B. Baranowski, M. K. Flatau, P. J. Flatau, and A. J. Matthews. Phase locking between atmospheric convectively coupled equatorial Kelvin waves and the diurnal cycle of precipitation over the Maritime Continent. *Geophysical Research Letters*, 43(15):8269–8276, 2016b. doi: <https://doi.org/10.1002/2016GL069602>. URL <https://agupubs.onlinelibrary.wiley.com/doi/abs/10.1002/2016GL069602>.

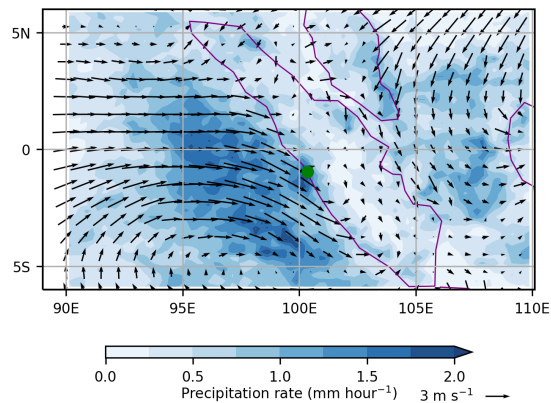


FIGURE 2 Composite TRMM precipitation rate and ERA5 surface wind vectors for extreme precipitation days at Padang when there is a CCKW present at $\tau = 6$ hours, where τ is the lag from 00:00 UTC on the day of extreme precipitation. Precipitation rate is colour shaded in blue (interval $0.25 \text{ mm hour}^{-1}$). The standard wind vector is 3 m s^{-1} . The location of Padang is shown by the green filled circle.

- D. B. Baranowski, M. K. Flatau, and P. J. Flatau. Social-media and newspaper reports reveal large-scale meteorological drivers of floods on Sumatra. *Nature Communications*, 11:2503, 2020. doi: 10.1038/s41467-020-16171-2.
- C. E. Birch, M. J. Roberts, L. Garcia-Carreras, D. Ackerley, M. J. Reeder, A. P. Lock, and R. Schiemann. Sea-Breeze Dynamics and Convection Initiation: The Influence of Convective Parameterization in Weather and Climate Model Biases. *Journal of Climate*, 28(20):8093 – 8108, 2015. doi: 10.1175/JCLI-D-14-00850.1. URL <https://journals.ametsoc.org/view/journals/clim/28/20/jcli-d-14-00850.1.xml>.
- J. E. Blanco, D. S. Nolan, and B. E. Mapes. Convectively coupled Kelvin waves in aquachannel simulations: 2. Life cycle and dynamical-convective coupling. *Journal of Geophysical Research: Atmospheres*, 121(19):11,319–11,347, 2016. doi: <https://doi.org/10.1002/2016JD025022>. URL <https://agupubs.onlinelibrary.wiley.com/doi/abs/10.1002/2016JD025022>.
- M. Bush, T. Allen, C. Bain, I. Boutle, J. Edwards, A. Finnenkoetter, C. Franklin, K. Hanley, H. Lean, A. Lock, J. Manners, M. Mittermaier, C. Morcrette, R. North, J. Petch, C. Short, S. Vosper, D. Walters, S. Webster, M. Weeks, J. Wilkinson, N. Wood, and M. Zerroukat. The first Met Office Unified Model–JULES Regional Atmosphere and Land configuration, RAL1. *Geoscientific Model Development*, 13(4):1999–2029, 2020. doi: 10.5194/gmd-13-1999-2020. URL <https://gmd.copernicus.org/articles/13/1999/2020/>.
- N. A. Da Silva and A. J. Matthews. Impact of the Madden–Julian Oscillation on extreme precipitation over the western Maritime Continent and Southeast Asia. *Quarterly Journal of the Royal Meteorological Society*, 147(739):3434–3453, 2021. doi: <https://doi.org/10.1002/qj.4136>. URL <https://rmets.onlinelibrary.wiley.com/doi/abs/10.1002/qj.4136>.
- J. Dias, M. Gehne, G. N. Kiladis, N. Sakaeda, P. Bechtold, and T. Haiden. Equatorial waves and the skill of ncep and ecmwf numerical weather prediction systems. *Monthly Weather Review*, 146(6):1763 – 1784, 2018. doi: 10.1175/MWR-D-17-0362.1. URL <https://journals.ametsoc.org/view/journals/mwre/146/6/mwr-d-17-0362.1.xml>.
- S. Ferrett, G.-Y. Yang, S. J. Woolnough, J. Methven, K. Hodges, and C. E. Holloway. Linking extreme precipitation in Southeast Asia to equatorial waves. *Quarterly Journal of the Royal Meteorological Society*, 146(727):665–684, 2020. doi: <https://doi.org/10.1002/qj.3699>. URL <https://rmets.onlinelibrary.wiley.com/doi/abs/10.1002/qj.3699>.
- P. R. Field, A. Hill, B. Shipway, K. Furtado, J. Wilkinson, A. Miltenberger, H. Gordon, D. P. Grosvenor, R. Stevens, and K. Van Weverberg. Implementation of a double moment cloud microphysics scheme in the uk met office regional numerical

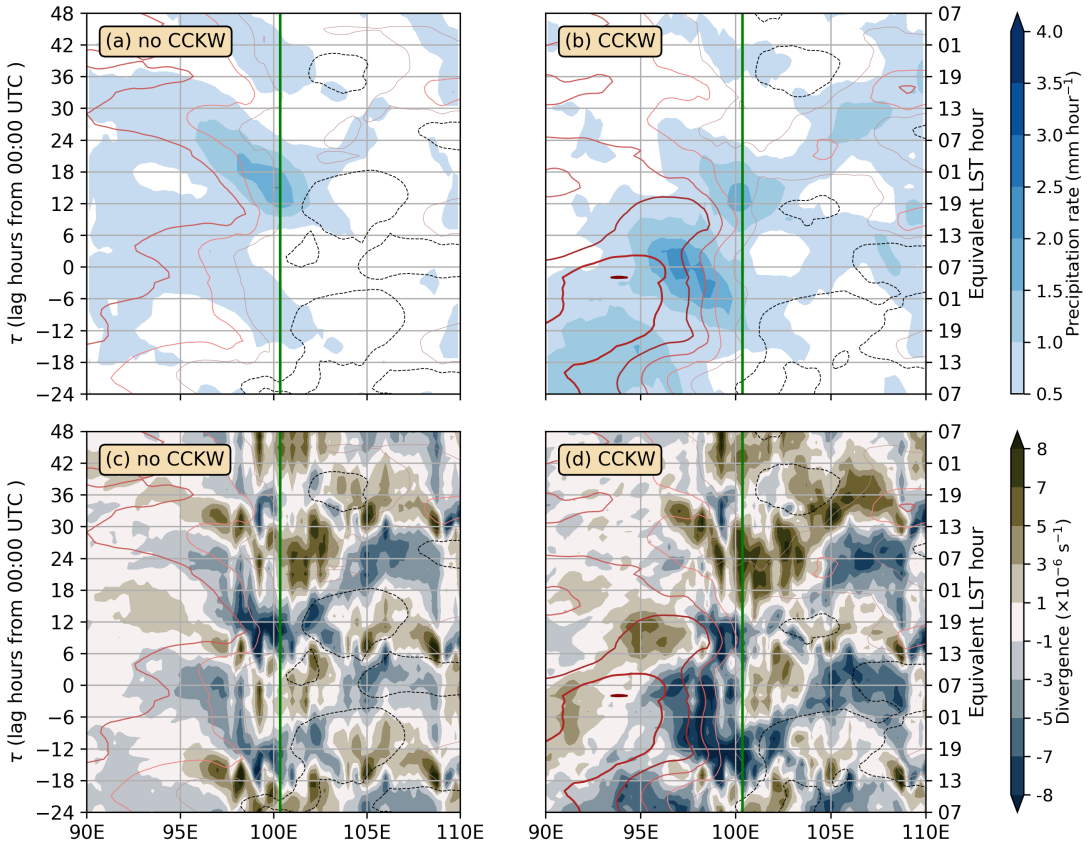


FIGURE 3 Composite Hovmöller diagram on extreme precipitation days at Padang, during the period 1998–2019 of TRMM precipitation rate (interval 0.5 mm hour^{-1}) when (a) no CCKW is present and (b) when a CCKW is present, and ERA5 975 hPa divergence (interval $1 \times 10^{-6} \text{ s}^{-1}$) when (c) a CCKW is not present and (d) when a CCKW is present. Data are averaged for 2.5°S – 2.5°N . The longitude of Padang is shown by a green line. The lag time τ is calculated from 00:00 UTC on day of extreme precipitation, the equivalent LST hour is indicated on the right side of the figure. ERA5 975 hPa zonal wind contours are drawn in red (interval 1 m s^{-1}) and the black dotted contour marks 0 m s^{-1} .

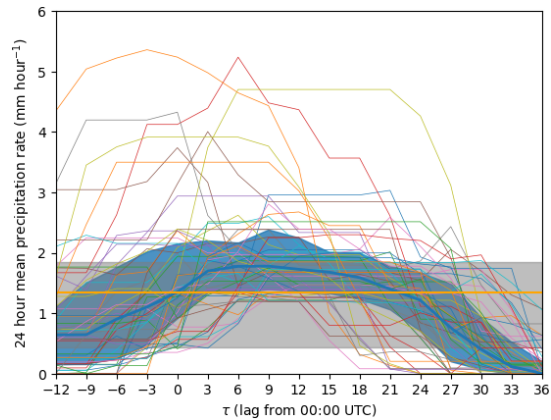


FIGURE 4 The 24 hour running-mean TRMM precipitation rate at Padang calculated over each day (± 12 hours) a CCKW has coincided with an extreme precipitation day (thin coloured lines), their median value (thick blue line) and their interquartile range (blue shading) are also given. The 95th percentile precipitation rate threshold (1.3 mm hour^{-1} ; thick orange line) and the interquartile range corresponding to the theoretical uniform distribution based on the mean 24 hour running-mean TRMM precipitation rate (grey shading) is also given. The 24 hour means are calculated as centered on lag time τ .

weather prediction model. *Quarterly Journal of the Royal Meteorological Society*, 149(752):703–739, 2023. doi: <https://doi.org/10.1002/qj.4414>. URL <https://rmets.onlinelibrary.wiley.com/doi/abs/10.1002/qj.4414>.

C M. Fine, R H. Johnson, P E. Ciesielski, and R K. Taft. The Role of Topographically Induced Vortices in Tropical Cyclone Formation over the Indian Ocean. *Monthly Weather Review*, 144(12):4827 – 4847, 2016. doi: 10.1175/MWR-D-16-0102.1. URL <https://journals.ametsoc.org/view/journals/mwre/144/12/mwr-d-16-0102.1.xml>.

O. S. Hai, A. A. Samah, S. N. Chenoli, K. Subramaniam, and M. Y. A. Mazuki. Extreme Rainstorms that Caused Devastating Flooding across the East Coast of Peninsular Malaysia during November and December 2014. *Weather and Forecasting*, 32(3):849 – 872, 2017. doi: 10.1175/WAF-D-16-0160.1. URL https://journals.ametsoc.org/view/journals/wefo/32/3/waf-d-16-0160_1.xml.

E. Hermawan, S. W. Lubis, T. Harjana, A. Purwaningsih, Risyanto, A Ridho, D F Andarini, D N Ratri, and R Widyaningsih. Large-Scale Meteorological Drivers of the Extreme Precipitation Event and Devastating Floods of Early-February 2021 in Semarang, Central Java, Indonesia. *Atmosphere*, 13(7), 2022. ISSN 2073-4433. doi: 10.3390/atmos13071092. URL <https://www.mdpi.com/2073-4433/13/7/1092>.

H. Hersbach, B. Bell, P. Berrisford, S. Hirahara, A. Horányi, J. Muñoz-Sabater, J. Nicolas, C. Peubey, R. Radu, D. Schepers, A. Simmons, C. Soci, S. Abdalla, X. Abellan, G. Balsamo, P. Bechtold, G. Biavati, J. Bidlot, M. Bonavita, G. De Chiara, P. Dahlgren, D. Dee, M. Diamantakis, R. Dragani, J. Flemming, R. Forbes, M. Fuentes, A. Geer, L. Haimberger, S. Healy, R. J. Hogan, E. Hólm, M. Janisková, S. Keeley, P. Laloyaux, P. Lopez, C. Lupu, G. Radnoti, P. de Rosnay, I. Rozum, F. Vamborg, S. Villaume, and J.-N. Thépaut. The ERA5 global reanalysis. *Quarterly Journal of the Royal Meteorological Society*, 146(730):1999–2049, 2020. doi: <https://doi.org/10.1002/qj.3803>. URL <https://rmets.onlinelibrary.wiley.com/doi/abs/10.1002/qj.3803>.

G. J. Huffman, R. F. Adler, D. T. Bolvin, and E. J. Nelkin. *The TRMM Multi-Satellite Precipitation Analysis (TMPA)*, pages 3–22. Springer Netherlands, Dordrecht, 2010. ISBN 978-90-481-2915-7. doi: 10.1007/978-90-481-2915-7_1. URL https://doi.org/10.1007/978-90-481-2915-7_1.

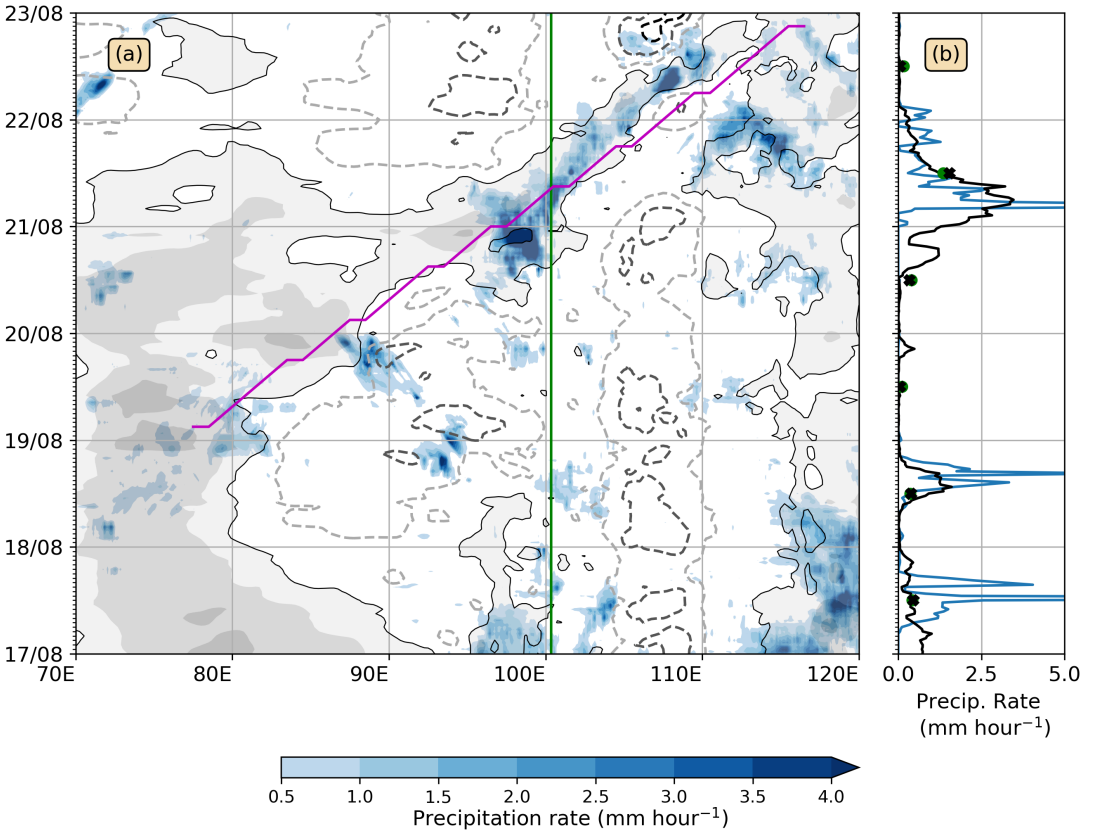


FIGURE 5 (a) Homöller diagram of IMERG precipitation (blue colour shading) and ERA5 10 m zonal wind (grey colour shading and line contours) for 17th–23rd August 2017 with time in UTC, averaged 2.5°S–2.5°N. (b) IMERG precipitation at Padang (blue) and the average over the 2°×2° box centered on Padang (black). The daily accumulated rainfall totals recorded by 113 stations (green filled circles) are compared to the daily integrated IMERG rainfall rates (black crosses) each averaged over the 2°×2° box centered on Padang. The longitude of Padang is shown by a green line in panel (a). ERA5 10 m zonal wind contours are drawn (interval 2 m s⁻¹). The first positive zonal wind shade (grey shading) is at 2 m s⁻¹ and first negative contour (grey dashed contour) at -2 m s⁻¹, with 0 m s⁻¹ marked with a solid black contour. The magenta line marks the observed CCKW trajectory.

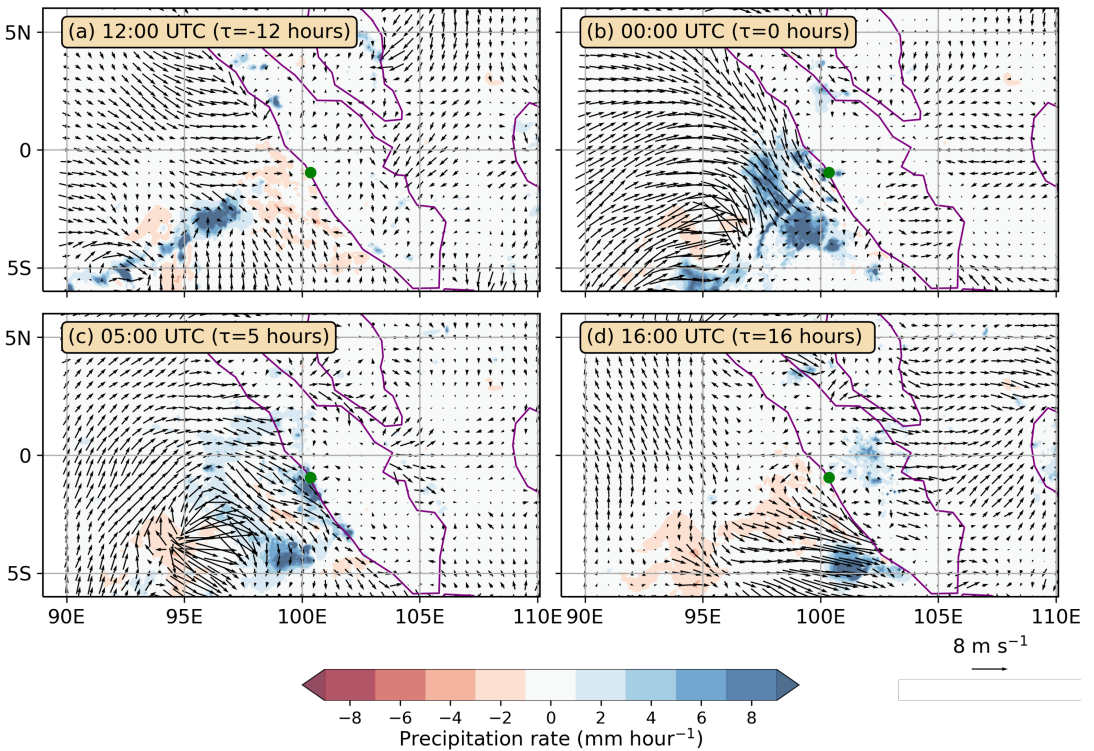


FIGURE 6 IMERG precipitation anomalies and anomalous ERA5 10 m wind vectors over Sumatra (arranged by increasing time) for (a) 20th August 2017 at 12:00 UTC, (b) 21st August 2017 at 00:00 UTC, (c) 21st August 2017 at 05:00 UTC and (d) 22nd August 2017 at 00:00 UTC. The equivalent lag time τ (lag from 00:00 UTC on the extreme precipitation day) is provided for comparison to the composite analysis. Anomalies calculated with respect to the 5 day mean period between 19th–23rd August 2017. Padang is shown by a green filled circle.

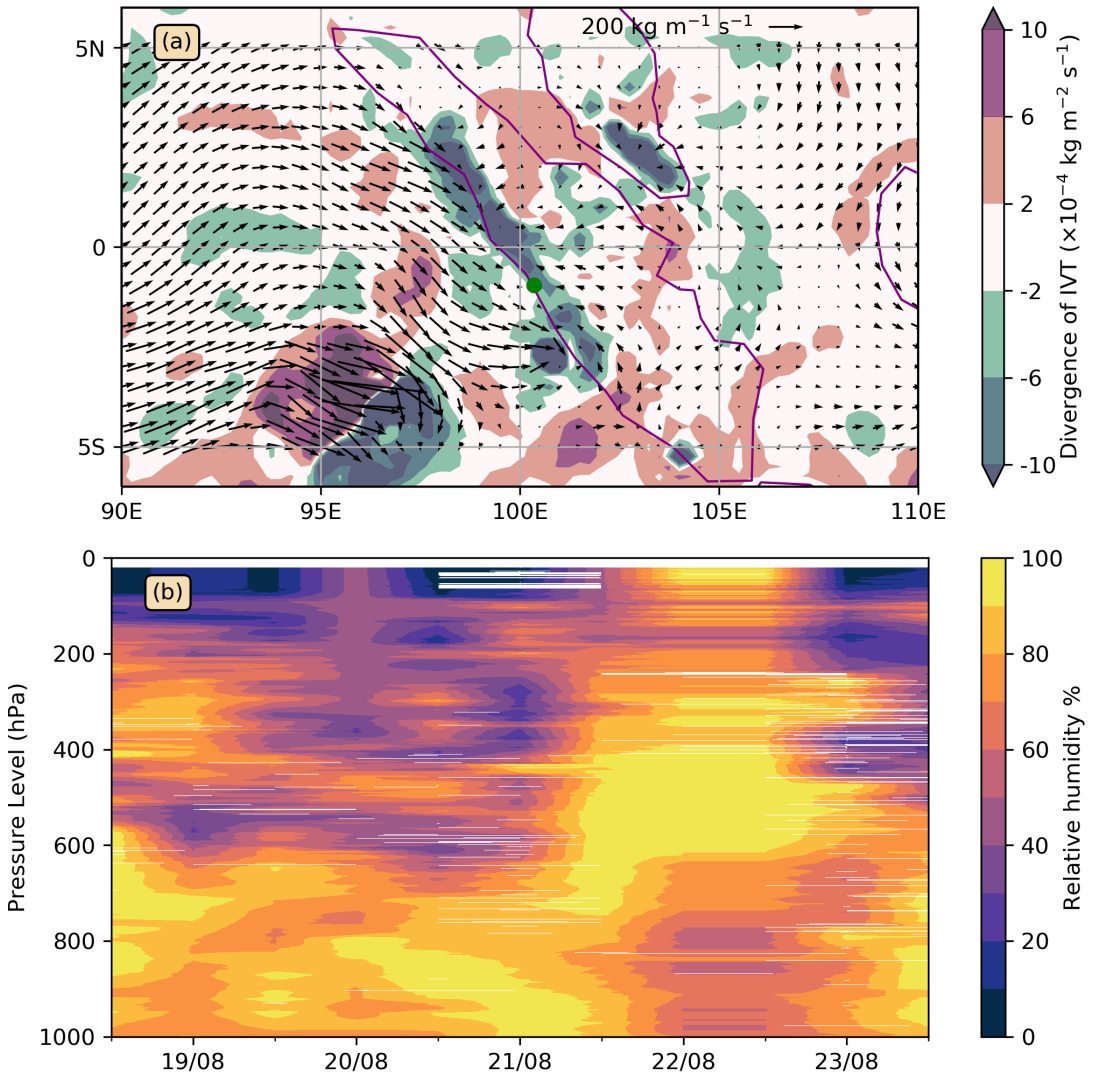


FIGURE 7 (

a) Vertically integrated moisture flux (IVT) anomalies from ERA5 (vectors) and IVT divergence (colour shading) at time of maximum precipitation at Padang (05:00 UTC on 21st August 2017). Anomalies are calculated with respect to the 5 day mean period between 19th–23rd August 2017. (b) Relative humidity measured using 12 hourly radiosonde ascents at Padang; date labels correspond to 00 UTC.

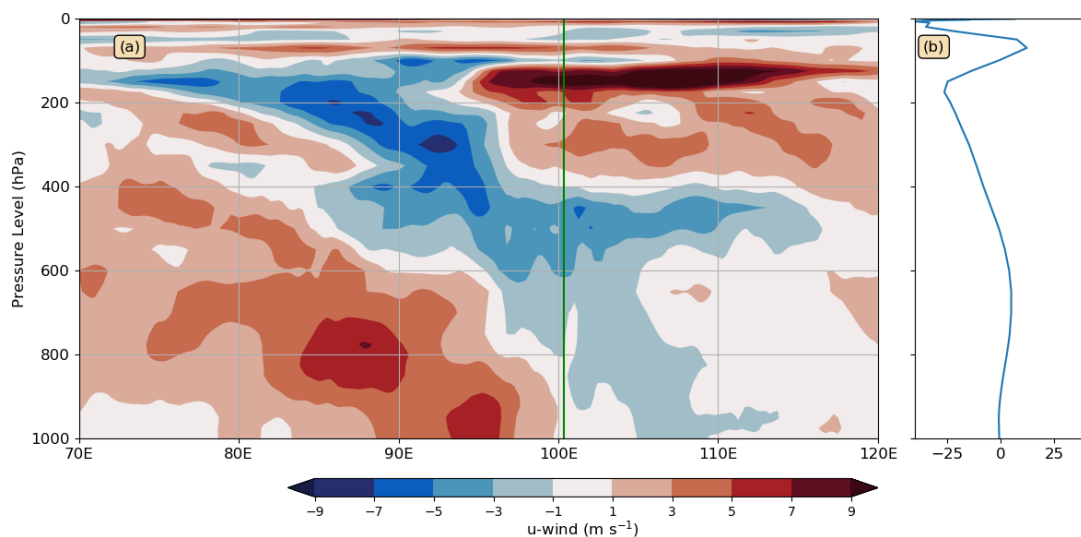


FIGURE 8 (a) Longitude–height section of the ERA5 zonal wind anomaly (averaged over 2.5°S – 2.5°N with interval 1 m s^{-1}) on 21st August 2017 at 00:00 UTC. The anomaly is calculated with respect to (b) the spatially averaged (2.5°S – 2.5°N , 70°E – 120°E), 5 day mean between 19th–23rd August 2017.

- George J Huffman, David T Bolvin, Eric J Nelkin, and Jackson Tan. Integrated Multi-satellite Retrievals for GPM (IMERG) technical documentation. Technical report, 2020. URL https://docsserver.gesdisc.eosdis.nasa.gov/public/project/GPM/IMERG_doc.06.pdf.
- G. W. Inverarity, W. J. Tennant, L. Anton, N. E. Bowler, A. M. Clayton, M. Jardak, A. C. Lorenc, F. Rawlins, S. A. Thompson, M. S. Thurlow, D. N. Walters, and M. A. Wlasak. Met Office MOGREPS-G initialisation using an ensemble of hybrid four-dimensional ensemble variational (En-4DnVar) data assimilations. *Quarterly Journal of the Royal Meteorological Society*, feb 2023. doi: 10.1002/qj.4431.
- W. S. Kessler, M. J. McPhaden, and K. M. Weickmann. Forcing of intraseasonal Kelvin waves in the equatorial Pacific. *Journal of Geophysical Research: Oceans*, 100(C6):10613–10631, 1995. doi: <https://doi.org/10.1029/95JC00382>. URL <https://agupubs.onlinelibrary.wiley.com/doi/abs/10.1029/95JC00382>.
- G. N. Kiladis, M. C. Wheeler, P. T. Haertel, K. H. Straub, and P. E. Roundy. Convectively coupled equatorial waves. *Reviews of Geophysics*, 47(2), 2009. doi: <https://doi.org/10.1029/2008RG000266>. URL <https://agupubs.onlinelibrary.wiley.com/doi/abs/10.1029/2008RG000266>.
- B. Latos, T. Lefort, M. K. Flatau, P. J. Flatau, D. S. Permana, D B. Baranowski, J A. I. Paski, E Makmur, E Sulystyo, P Peyrillé, Z Feng, A J. Matthews, and J M. Schmidt. Equatorial Waves Triggering Extreme Rainfall and Floods in Southwest Sulawesi, Indonesia. *Monthly Weather Review*, 149(5):1381 – 1401, 2021. doi: 10.1175/MWR-D-20-0262.1. URL <https://journals.ametsoc.org/view/journals/mwre/149/5/MWR-D-20-0262.1.xml>.
- B. S. Love, A. J. Matthews, and G. M. S. Lister. The diurnal cycle of precipitation over the Maritime Continent in a high-resolution atmospheric model. *Quarterly Journal of the Royal Meteorological Society*, 137(657):934–947, 2011. doi: <https://doi.org/10.1002/qj.809>. URL <https://rmets.onlinelibrary.wiley.com/doi/abs/10.1002/qj.809>.
- S. W. Lubis and M. R. Respati. Impacts of convectively coupled equatorial waves on rainfall extremes in Java, Indonesia. *International Journal of Climatology*, 41(4):2418–2440, 2021. doi: <https://doi.org/10.1002/joc.6967>. URL <https://rmets.onlinelibrary.wiley.com/doi/abs/10.1002/joc.6967>.

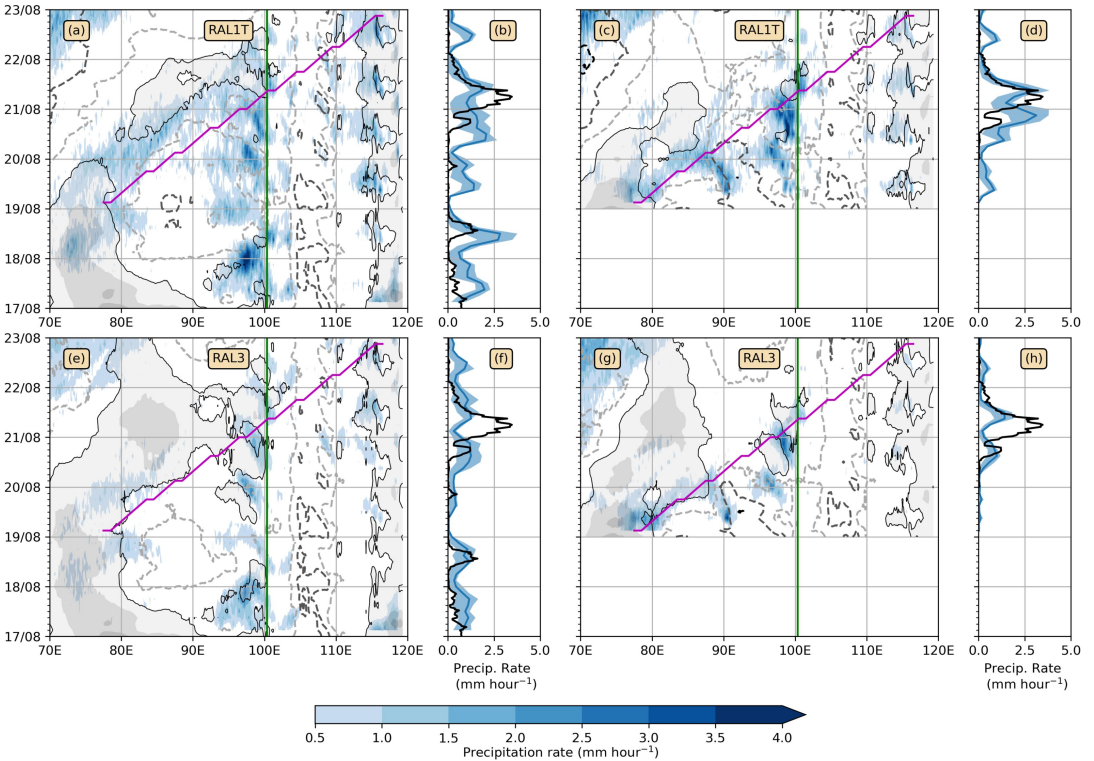


FIGURE 9 Hovmöller of ensemble-averaged precipitation rate for an ensemble of RAL1T forecasts initialised on (a) 17th August 2017 and (c) 19th August 2017, and an ensemble of RAL3 forecasts initialised on (e) 17th August 2017 and (g) 19th August 2017. (b), (d), (f), (h), are their ensemble mean precipitation rates over the $2^\circ \times 2^\circ$ box centred on Padang (blue) corresponding to (a), (c), (e) and (g) respectively. The blue shading represents the interquartile range and the $2^\circ \times 2^\circ$ average IMERG precipitation rate is shown in black. In (a), (c), (e), (g), zonal wind contours are drawn (interval 2 m s^{-1}). The first positive zonal wind shade (grey shading) is at 2 m s^{-1} and first negative contour (grey dashed contour) at -2 m s^{-1} , with 0 m s^{-1} marked with a solid black contour. The magenta line marks the observed CCKW trajectory. All forecasts have been initialised at 00:00 UTC. The Hovmöller diagrams have been latitude averaged between 2.5°S – 2.5°N .

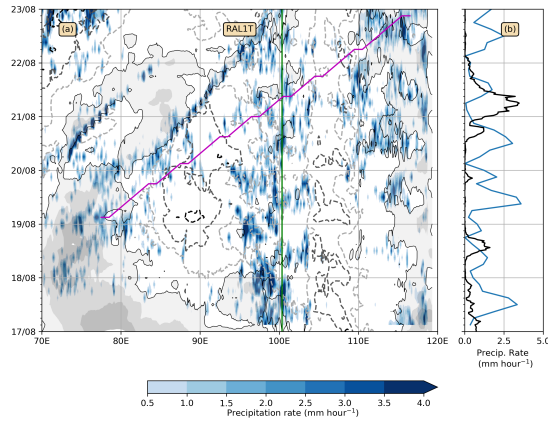


FIGURE 10 (a) Hovmöller of a single RAL1T ensemble member from a run initialised 17th August 2017 00:00 UTC, latitude averaged 2.5S–2.5N. (b) The simulated precipitation rate averaged over the $2^\circ \times 2^\circ$ box centred on Padang (blue) and that of the IMERG precipitation rate (black) is also shown. Zonal wind contours are drawn (interval 2 m s^{-1}). The first positive zonal wind shade (grey shading) is at 2 m s^{-1} and first negative contour (grey dashed contour) at -2 m s^{-1} , with 0 m s^{-1} marked with a solid black contour. The magenta line marks the observed CCKW trajectory.

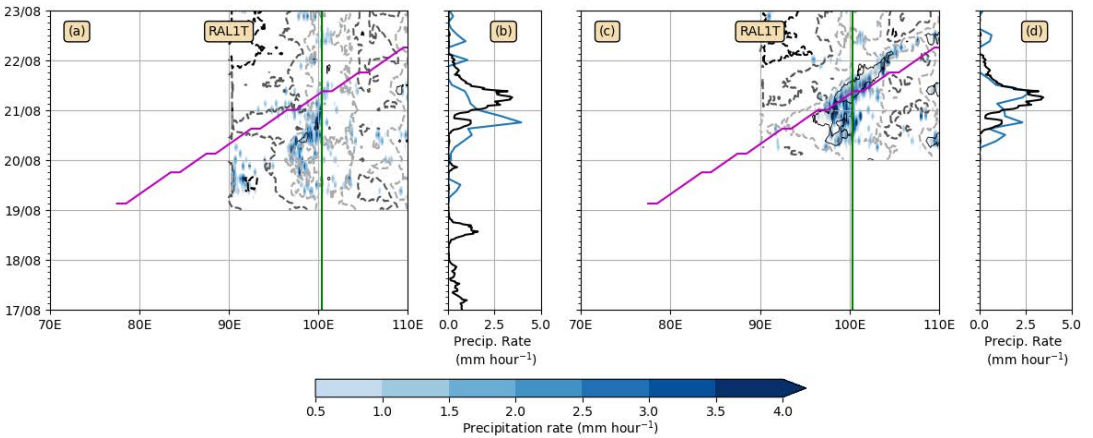


FIGURE 11 Hovmöller (latitude averaged 2.5°S – 2.5°N) of the SEA RAL1T deterministic 4.4 km model with western boundary at 90°E initialised on (a) 19th August 2017 00:00 UTC with (b) corresponding precipitation rate averaged over the $2^\circ \times 2^\circ$ box centred on Padang; (c) 20th August 2017 00:00 UTC with (d) corresponding precipitation rate averaged over the $2^\circ \times 2^\circ$ box centred on Padang. The longitude of Padang is marked with a green line. The first positive zonal wind shade (grey shading) is at 2 m s^{-1} and first negative contour (grey dashed contour) at -2 m s^{-1} , with 0 m s^{-1} marked with a solid black contour. The magenta line marks the observed CCKW trajectory.

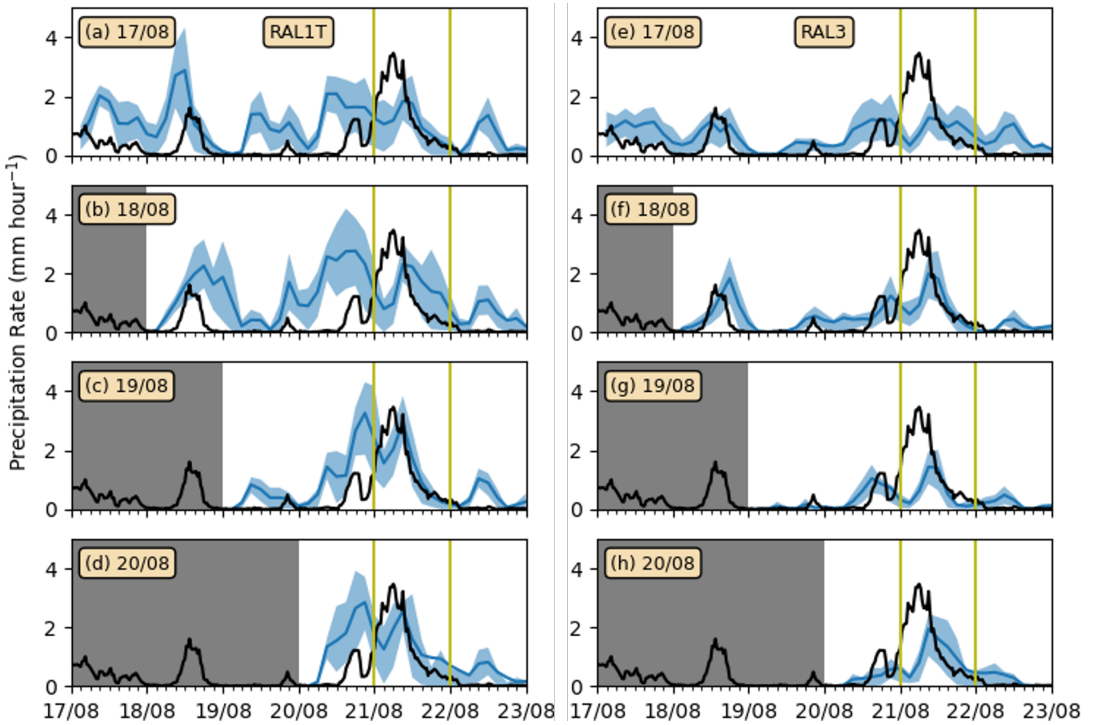


FIGURE 12 Ensemble averaged simulated precipitation rate (blue) and interquartile range (blue shading) spatially averaged over the $2^{\circ} \times 2^{\circ}$ box centered on Padang for RAL1T runs at initialisation times (a) 17th August 2017 00:00 UTC, (b) 18th August 2017 00:00 UTC, (c) 19th August 2017 00:00 UTC and (d) 20th August 2017 00:00 UTC. (e), (f), (g), (h) is the same as (a), (b), (c), (d) but for RAL3 runs. Observed (IMERG) precipitation rate averaged over the $2^{\circ} \times 2^{\circ}$ box is shown in black for comparison. Grey shading marks the region where the run has not yet initialised. The two lime-green lines mark the start and end of the extreme precipitation day (21st August 2017).

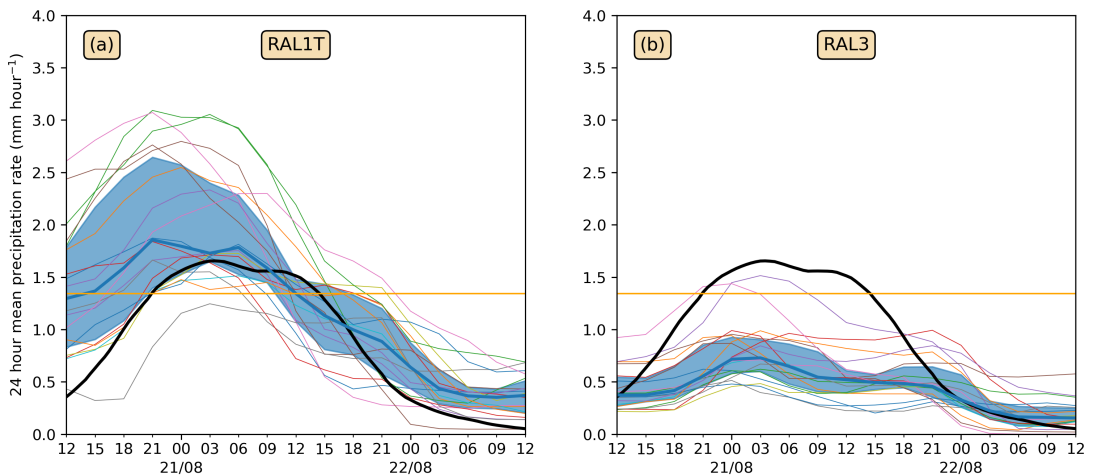


FIGURE 13 24 hour running-mean simulated precipitation rates of an ensembles of runs initialised on 19th August 2017 00:00 UTC in the (a) RAL1T and (b) RA3 configuration. These are spatially averaged over the $2^\circ \times 2^\circ$ box centered on Padang. Each ensemble member is shown (thin coloured lines) as well as their median values (thick blue) and their interquartile range (blue shading). The observed 24 hour running-mean (IMERG) precipitation rate averaged over the $2^\circ \times 2^\circ$ box centered on Padang is also provided for reference (thick black). The 95th percentile extreme precipitation threshold value of 1.3 mm hour^{-1} is denoted by the orange line. The 24 hour means are calculated as centered on the hour.

- A. J. Matthews. Dynamical propagation and growth mechanisms for convectively coupled equatorial Kelvin waves over the Indian Ocean. *Quarterly Journal of the Royal Meteorological Society*, 147(741):4310–4336, 2021. doi: <https://doi.org/10.1002/qj.4179>. URL <https://rsmets.onlinelibrary.wiley.com/doi/abs/10.1002/qj.4179>.
- M. B. Menary, T. Kuhlbrodt, J. Ridley, M. B. Andrews, O. B. Dimdore-Miles, J. Deshayes, R. Eade, L. Gray, S. Ineson, J. Mignot, C. D. Roberts, J. Robson, R. A. Wood, and P. Xavier. Preindustrial Control Simulations With HadGEM3-GC3.1 for CMIP6. *Journal of Advances in Modeling Earth Systems*, 10(12):3049–3075, 2018. doi: <https://doi.org/10.1029/2018MS001495>. URL <https://agupubs.onlinelibrary.wiley.com/doi/abs/10.1029/2018MS001495>.
- T. Nakazawa. Tropical Super Clusters within Intraseasonal Variations over the Western Pacific. *Journal of the Meteorological Society of Japan. Ser. II*, 66(6):823–839, 1988. doi: 10.2151/jmsj1965.66.6_823.
- S. C. Peatman, A. J. Matthews, and D. P. Stevens. Propagation of the Madden–Julian Oscillation through the Maritime Continent and scale interaction with the diurnal cycle of precipitation. *Quarterly Journal of the Royal Meteorological Society*, 140(680):814–825, 2014. doi: 10.1002/qj.2161.
- S. C. Peatman, J. Schwendike, C. E. Birch, J. H. Marsham, A. J. Matthews, and G.-Y. Yang. A Local-to-Large Scale View of Maritime Continent Rainfall: Control by ENSO, MJO, and Equatorial Waves. *Journal of Climate*, 34(22):8933 – 8953, 2021. doi: 10.1175/JCLI-D-21-0263.1. URL <https://journals.ametsoc.org/view/journals/clim/34/22/JCLI-D-21-0263.1.xml>.
- A. F. Prein, W. Langhans, G. Fosser, A. Ferrone, N. Ban, K. Goergen, M. Keller, M. Tölle, O. Gutjahr, F. Feser, E. Brisson, S. Kollet, J. Schmidli, N. P. M. van Lipzig, and R. Leung. A review on regional convection-permitting climate modeling: Demonstrations, prospects, and challenges. *Reviews of Geophysics*, 53(2):323–361, 2015. doi: <https://doi.org/10.1002/2014RG000475>. URL <https://agupubs.onlinelibrary.wiley.com/doi/abs/10.1002/2014RG000475>.
- A. Purwaningsih, S. W. Lubis, E. Hermawan, D. F. Andarini, T. Harjana, D. N. Ratri, A. Ridho, Risyanto, and A. P. Sujalu. Moisture Origin and Transport for Extreme Precipitation over Indonesia’s New Capital City, Nusantara in August 2021. *Atmosphere*, 13(9), 2022. ISSN 2073-4433. doi: 10.3390/atmos13091391. URL <https://www.mdpi.com/2073-4433/13/9/1391>.

- J.-H. Qian. Why Precipitation Is Mostly Concentrated over Islands in the Maritime Continent. *Journal of the Atmospheric Sciences*, 65(4):1428 – 1441, 2008. doi: 10.1175/2007JAS2422.1. URL <https://journals.ametsoc.org/view/journals/atsc/65/4/2007jas2422.1.xml>.
- C. S. Ramage. Role of a tropical "Maritime Continent" in the atmospheric circulation. *Monthly Weather Review*, 96(6):365 – 370, 1968. doi: 10.1175/1520-0493(1968)096<0365:ROATMC>2.0.CO;2. URL https://journals.ametsoc.org/view/journals/mwre/96/6/1520-0493_1968_096_0365_roatmc_2_0_co_2.xml.
- M. J. Roberts, A. Baker, E. W. Blockley, D. Calvert, A. Coward, H. T. Hewitt, L. C. Jackson, T. Kuhlbrodt, P. Mathiot, C. D. Roberts, R. Schiemann, J. Seddon, B. Vannière, and P. L. Vidale. Description of the resolution hierarchy of the global coupled HadGEM3-GC3.1 model as used in CMIP6 HighResMIP experiments. *Geoscientific Model Development*, 12(12): 4999–5028, 2019. doi: 10.5194/gmd-12-4999-2019. URL <https://gmd.copernicus.org/articles/12/4999/2019/>.
- P. E. Roundy. Analysis of Convectively Coupled Kelvin Waves in the Indian Ocean MJO. *Journal of the Atmospheric Sciences*, 65(4):1342 – 1359, 2008. doi: 10.1175/2007JAS2345.1. URL <https://journals.ametsoc.org/view/journals/atsc/65/4/2007jas2345.1.xml>.
- N. Sakaeda, G. Kiladis, and J. Dias. The Diurnal Cycle of Rainfall and the Convectively Coupled Equatorial Waves over the Maritime Continent. *Journal of Climate*, 33(8):3307 – 3331, 2020. doi: 10.1175/JCLI-D-19-0043.1. URL <https://journals.ametsoc.org/view/journals/clim/33/8/jcli-d-19-0043.1.xml>.
- E. Short, C. L. Vincent, and T. P. Lane. Diurnal Cycle of Surface Winds in the Maritime Continent Observed through Satellite Scatterometry. *Monthly Weather Review*, 147(6):2023 – 2044, 2019. doi: 10.1175/MWR-D-18-0433.1. URL <https://journals.ametsoc.org/view/journals/mwre/147/6/mwr-d-18-0433.1.xml>.
- K. H. Straub and G. N. Kiladis. The Observed Structure of Convectively Coupled Kelvin Waves: Comparison with Simple Models of Coupled Wave Instability. *Journal of the Atmospheric Sciences*, 60(14):1655 – 1668, 2003. doi: 10.1175/1520-0469(2003)060<1655:TOSOCC>2.0.CO;2. URL https://journals.ametsoc.org/view/journals/atsc/60/14/1520-0469_2003_060_1655_tosocc_2_0_co_2.xml.
- R. van der Linden, A. H. Fink, J. G. Pinto, T. Phan-Van, and G. N. Kiladis. Modulation of Daily Rainfall in Southern Vietnam by the Madden–Julian Oscillation and Convectively Coupled Equatorial Waves. *Journal of Climate*, 29(16):5801 – 5820, 2016. doi: 10.1175/JCLI-D-15-0911.1. URL <https://journals.ametsoc.org/view/journals/clim/29/16/jcli-d-15-0911.1.xml>.
- K. Van Weverberg, C. J. Morcrette, I. Boutle, K. Furtado, and P. R. Field. A Bimodal Diagnostic Cloud Fraction Parameterization. Part I: Motivating Analysis and Scheme Description. *Monthly Weather Review*, 149(3):841 – 857, 2021. doi: 10.1175/MWR-D-20-0224.1. URL <https://journals.ametsoc.org/view/journals/mwre/149/3/MWR-D-20-0224.1.xml>.
- C. L. Vincent, T. P. Lane, and M. C. Wheeler. A local index of Maritime Continent intraseasonal variability based on rain rates over the land and sea. *Geophysical Research Letters*, 43(17):9306–9314, 2016. doi: <https://doi.org/10.1002/2016GL069987>. URL <https://agupubs.onlinelibrary.wiley.com/doi/abs/10.1002/2016GL069987>.
- D. Walters, I. Boutle, M. Brooks, T. Melvin, R. Stratton, S. Vosper, H. Wells, K. Williams, N. Wood, T. Allen, A. Bushell, D. Copesey, P. Earnshaw, J. Edwards, M. Gross, S. Hardiman, C. Harris, J. Heming, N. Klingaman, R. Levine, J. Manners, G. Martin, S. Milton, M. Mittermaier, C. Morcrette, T. Riddick, M. Roberts, C. Sanchez, P. Selwood, A. Stirling, C. Smith, D. Suri, W. Tennant, P. L. Vidale, J. Wilkinson, M. Willett, S. Woolnough, and P. Xavier. The Met Office Unified Model Global Atmosphere 6.0/6.1 and JULES Global Land 6.0/6.1 configurations. *Geoscientific Model Development*, 10(4):1487–1520, 2017. doi: 10.5194/gmd-10-1487-2017. URL <https://gmd.copernicus.org/articles/10/1487/2017/>.
- M. Wheeler and G. N. Kiladis. Convectively Coupled Equatorial Waves: Analysis of Clouds and Temperature in the Wavenumber–Frequency Domain. *Journal of the Atmospheric Sciences*, 56(3):374 – 399, 1999. doi: 10.1175/1520-0469(1999)056<0374:CCEWAO>2.0.CO;2. URL https://journals.ametsoc.org/view/journals/atsc/56/3/1520-0469_1999_056_0374_ccewao_2_0_co_2.xml.

- K. D. Williams, D. Copley, E. W. Blockley, A. Bodas-Salcedo, D. Calvert, R. Comer, P. Davis, T. Graham, H. T. Hewitt, R. Hill, P. Hyder, S. Ineson, T. C. Johns, A. B. Keen, R. W. Lee, A. Megann, S. F. Milton, J. G. L. Rae, M. J. Roberts, A. A. Scaife, R. Schiemann, D. Storkey, L. Thorpe, I. G. Watterson, D. N. Walters, A. West, R. A. Wood, T. Woollings, and P. K. Xavier. The Met Office Global Coupled Model 3.0 and 3.1 (GC3.0 and GC3.1) Configurations. *Journal of Advances in Modeling Earth Systems*, 10(2):357–380, 2018. doi: <https://doi.org/10.1002/2017MS001115>. URL <https://agupubs.onlinelibrary.wiley.com/doi/abs/10.1002/2017MS001115>.
- D. R. Wilson and S. P. Ballard. A microphysically based precipitation scheme for the UK meteorological office unified model. *Quarterly Journal of the Royal Meteorological Society*, 125(557):1607–1636, 1999. doi: <https://doi.org/10.1002/qj.49712555707>. URL <https://rmets.onlinelibrary.wiley.com/doi/abs/10.1002/qj.49712555707>.
- D. R. Wilson, A. C. Bushell, A. M. Kerr-Munslow, J. D. Price, and C. J. Morcrette. PC2: A prognostic cloud fraction and condensation scheme. I: Scheme description. *Quarterly Journal of the Royal Meteorological Society*, 134(637):2093–2107, 2008. doi: <https://doi.org/10.1002/qj.333>. URL <https://rmets.onlinelibrary.wiley.com/doi/abs/10.1002/qj.333>.
- P. Wu, M. Hara, J-i Hamada, M. D. Yamanaka, and F. Kimura. Why a Large Amount of Rain Falls over the Sea in the Vicinity of Western Sumatra Island during Nighttime. *Journal of Applied Meteorology and Climatology*, 48(7):1345 – 1361, 2009. doi: [10.1175/2009JAMC2052.1](https://doi.org/10.1175/2009JAMC2052.1). URL <https://journals.ametsoc.org/view/journals/apme/48/7/2009jamc2052.1.xml>.
- G.-Y. Yang and Julia Slingo. The Diurnal Cycle in the Tropics. *Monthly Weather Review*, 129(4):784 – 801, 2001. doi: [10.1175/1520-0493\(2001\)129<0784:TDCITT>2.0.CO;2](https://doi.org/10.1175/1520-0493(2001)129<0784:TDCITT>2.0.CO;2). URL https://journals.ametsoc.org/view/journals/mwre/129/4/1520-0493_2001_129_0784_tdcitt_2.0.co_2.xml.

references

- R. Akbar. Diguyur Hujan dari Pagi, Ratusan Rumah di Padang Pariaman Terendam Banjir 1,5 Meter. *Okezone*, 2017. URL <https://news.okezone.com/read/2017/08/21/340/1759869/diguyur-hujan-dari-pagi-ratusan-rumah-di-padang-pariaman-terendam-banjir-1-5-meter>.
- H. Bai, G. Deranadyan, C. Schumacher, A. Funk, C. Epifanio, A. Ali, Endarwin, F. Radjab, R. Adriyanto, N. Nurhayati, Y. Nugraha, and A. Fauziah. Formation of Nocturnal Offshore Rainfall near the West Coast of Sumatra: Land Breeze or Gravity Wave? *Monthly Weather Review*, 149(3):715 – 731, 2021. doi: [10.1175/MWR-D-20-0179.1](https://doi.org/10.1175/MWR-D-20-0179.1). URL <https://journals.ametsoc.org/view/journals/mwre/149/3/MWR-D-20-0179.1.xml>.
- D. B. Baranowski, M. K. Flatau, P. J. Flatau, and A. J. Matthews. Impact of atmospheric convectively coupled equatorial Kelvin waves on upper ocean variability. *Journal of Geophysical Research: Atmospheres*, 121(5):2045–2059, 2016a. doi: <https://doi.org/10.1002/2015JD024150>. URL <https://agupubs.onlinelibrary.wiley.com/doi/abs/10.1002/2015JD024150>.
- D. B. Baranowski, M. K. Flatau, P. J. Flatau, and A. J. Matthews. Phase locking between atmospheric convectively coupled equatorial Kelvin waves and the diurnal cycle of precipitation over the Maritime Continent. *Geophysical Research Letters*, 43(15):8269–8276, 2016b. doi: <https://doi.org/10.1002/2016GL069602>. URL <https://agupubs.onlinelibrary.wiley.com/doi/abs/10.1002/2016GL069602>.
- D. B. Baranowski, M. K. Flatau, and P. J. Flatau. Social-media and newspaper reports reveal large-scale meteorological drivers of floods on Sumatra. *Nature Communications*, 11:2503, 2020. doi: [10.1038/s41467-020-16171-2](https://doi.org/10.1038/s41467-020-16171-2).
- C. E. Birch, M. J. Roberts, L. Garcia-Carreras, D. Ackerley, M. J. Reeder, A. P. Lock, and R. Schiemann. Sea-Breeze Dynamics and Convection Initiation: The Influence of Convective Parameterization in Weather and Climate Model Biases. *Journal of Climate*, 28(20):8093 – 8108, 2015. doi: [10.1175/JCLI-D-14-00850.1](https://doi.org/10.1175/JCLI-D-14-00850.1). URL <https://journals.ametsoc.org/view/journals/clim/28/20/jcli-d-14-00850.1.xml>.
- J. E. Blanco, D. S. Nolan, and B. E. Mapes. Convectively coupled Kelvin waves in aquachannel simulations: 2. Life cycle and dynamical-convective coupling. *Journal of Geophysical Research: Atmospheres*, 121(19):11,319–11,347, 2016. doi: <https://doi.org/10.1002/2016JD025022>. URL <https://agupubs.onlinelibrary.wiley.com/doi/abs/10.1002/2016JD025022>.

- M. Bush, T. Allen, C. Bain, I. Boutle, J. Edwards, A. Finnenkoetter, C. Franklin, K. Hanley, H. Lean, A. Lock, J. Manners, M. Mittermaier, C. Morcrette, R. North, J. Petch, C. Short, S. Vosper, D. Walters, S. Webster, M. Weeks, J. Wilkinson, N. Wood, and M. Zerroukat. The first Met Office Unified Model–JULES Regional Atmosphere and Land configuration, RAL1. *Geoscientific Model Development*, 13(4):1999–2029, 2020. doi: 10.5194/gmd-13-1999-2020. URL <https://gmd.copernicus.org/articles/13/1999/2020/>.
- N. A. Da Silva and A. J. Matthews. Impact of the Madden–Julian Oscillation on extreme precipitation over the western Maritime Continent and Southeast Asia. *Quarterly Journal of the Royal Meteorological Society*, 147(739):3434–3453, 2021. doi: <https://doi.org/10.1002/qj.4136>. URL <https://rmets.onlinelibrary.wiley.com/doi/abs/10.1002/qj.4136>.
- J. Dias, M. Gehne, G. N. Kiladis, N. Sakaeda, P. Bechtold, and T. Haiden. Equatorial waves and the skill of ncep and ecmwf numerical weather prediction systems. *Monthly Weather Review*, 146(6):1763 – 1784, 2018. doi: 10.1175/MWR-D-17-0362.1. URL <https://journals.ametsoc.org/view/journals/mwre/146/6/mwr-d-17-0362.1.xml>.
- S. Ferrett, G.-Y. Yang, S. J. Woolnough, J. Methven, K. Hodges, and C. E. Holloway. Linking extreme precipitation in Southeast Asia to equatorial waves. *Quarterly Journal of the Royal Meteorological Society*, 146(727):665–684, 2020. doi: <https://doi.org/10.1002/qj.3699>. URL <https://rmets.onlinelibrary.wiley.com/doi/abs/10.1002/qj.3699>.
- P. R. Field, A. Hill, B. Shipway, K. Furtado, J. Wilkinson, A. Miltenberger, H. Gordon, D. P. Grosvenor, R. Stevens, and K. Van Weverberg. Implementation of a double moment cloud microphysics scheme in the uk met office regional numerical weather prediction model. *Quarterly Journal of the Royal Meteorological Society*, 149(752):703–739, 2023. doi: <https://doi.org/10.1002/qj.4414>. URL <https://rmets.onlinelibrary.wiley.com/doi/abs/10.1002/qj.4414>.
- C M. Fine, R H. Johnson, P E. Ciesielski, and R K. Taft. The Role of Topographically Induced Vortices in Tropical Cyclone Formation over the Indian Ocean. *Monthly Weather Review*, 144(12):4827 – 4847, 2016. doi: 10.1175/MWR-D-16-0102.1. URL <https://journals.ametsoc.org/view/journals/mwre/144/12/mwr-d-16-0102.1.xml>.
- O. S. Hai, A. A. Samah, S. N. Chenoli, K. Subramaniam, and M. Y. A. Mazuki. Extreme Rainstorms that Caused Devastating Flooding across the East Coast of Peninsular Malaysia during November and December 2014. *Weather and Forecasting*, 32(3):849 – 872, 2017. doi: 10.1175/WAF-D-16-0160.1. URL https://journals.ametsoc.org/view/journals/wefo/32/3/waf-d-16-0160_1.xml.
- E. Hermawan, S. W. Lubis, T. Harjana, A. Purwaningsih, Risyanto, A Ridho, D F Andarini, D N Ratri, and R Widyaningsih. Large-Scale Meteorological Drivers of the Extreme Precipitation Event and Devastating Floods of Early-February 2021 in Semarang, Central Java, Indonesia. *Atmosphere*, 13(7), 2022. ISSN 2073-4433. doi: 10.3390/atmos13071092. URL <https://www.mdpi.com/2073-4433/13/7/1092>.
- H. Hersbach, B. Bell, P. Berrisford, S. Hirahara, A. Horányi, J. Muñoz-Sabater, J. Nicolas, C. Peubey, R. Radu, D. Schepers, A. Simmons, C. Soci, S. Abdalla, X. Abellan, G. Balsamo, P. Bechtold, G. Biavati, J. Bidlot, M. Bonavita, G. De Chiara, P. Dahlgren, D. Dee, M. Diamantakis, R. Dragani, J. Flemming, R. Forbes, M. Fuentes, A. Geer, L. Haimberger, S. Healy, R. J. Hogan, E. Hólm, M. Janisková, S. Keeley, P. Laloyaux, P. Lopez, C. Lupu, G. Radnoti, P. de Rosnay, I. Rozum, F. Vamborg, S. Villaume, and J.-N. Thépaut. The ERA5 global reanalysis. *Quarterly Journal of the Royal Meteorological Society*, 146(730):1999–2049, 2020. doi: <https://doi.org/10.1002/qj.3803>. URL <https://rmets.onlinelibrary.wiley.com/doi/abs/10.1002/qj.3803>.
- G. J. Huffman, R. F. Adler, D. T. Bolvin, and E. J. Nelkin. *The TRMM Multi-Satellite Precipitation Analysis (TMPA)*, pages 3–22. Springer Netherlands, Dordrecht, 2010. ISBN 978-90-481-2915-7. doi: 10.1007/978-90-481-2915-7_1. URL https://doi.org/10.1007/978-90-481-2915-7_1.
- George J Huffman, David T Bolvin, Eric J Nelkin, and Jackson Tan. Integrated Multi-satellite Retrievals for GPM (IMERG) technical documentation. Technical report, 2020. URL https://docserver.gesdisc.eosdis.nasa.gov/public/project/GPM/IMERG_doc.06.pdf.
- G. W. Inverarity, W. J. Tennant, L. Anton, N. E. Bowler, A. M. Clayton, M. Jardak, A. C. Lorenc, F. Rawlins, S. A. Thompson, M. S. Thurlow, D. N. Walters, and M. A. Wlasak. Met Office MOGREPS-G initialisation using an ensemble of hybrid four-dimensional ensemble variational (En-4DnVar) data assimilations. *Quarterly Journal of the Royal Meteorological Society*, feb 2023. doi: 10.1002/qj.4431.

- W. S. Kessler, M. J. McPhaden, and K. M. Weickmann. Forcing of intraseasonal Kelvin waves in the equatorial Pacific. Journal of Geophysical Research: Oceans, 100(C6):10613–10631, 1995. doi: <https://doi.org/10.1029/95JC00382>. URL <https://agupubs.onlinelibrary.wiley.com/doi/abs/10.1029/95JC00382>.
- G. N. Kiladis, M. C. Wheeler, P. T. Haertel, K. H. Straub, and P. E. Roundy. Convectively coupled equatorial waves. Reviews of Geophysics, 47(2), 2009. doi: <https://doi.org/10.1029/2008RG000266>. URL <https://agupubs.onlinelibrary.wiley.com/doi/abs/10.1029/2008RG000266>.
- B. Latos, T. Lefort, M. K. Flatau, P. J. Flatau, D. S. Permana, D. B. Baranowski, J. A. I. Paski, E. Makmur, E. Sulystyo, P. Peyrillé, Z. Feng, A. J. Matthews, and J. M. Schmidt. Equatorial Waves Triggering Extreme Rainfall and Floods in Southwest Sulawesi, Indonesia. Monthly Weather Review, 149(5):1381 – 1401, 2021. doi: 10.1175/MWR-D-20-0262.1. URL <https://journals.ametsoc.org/view/journals/mwre/149/5/MWR-D-20-0262.1.xml>.
- B. S. Love, A. J. Matthews, and G. M. S. Lister. The diurnal cycle of precipitation over the Maritime Continent in a high-resolution atmospheric model. Quarterly Journal of the Royal Meteorological Society, 137(657):934–947, 2011. doi: <https://doi.org/10.1002/qj.809>. URL <https://rmets.onlinelibrary.wiley.com/doi/abs/10.1002/qj.809>.
- S. W. Lubis and M. R. Respati. Impacts of convectively coupled equatorial waves on rainfall extremes in Java, Indonesia. International Journal of Climatology, 41(4):2418–2440, 2021. doi: <https://doi.org/10.1002/joc.6967>. URL <https://rmets.onlinelibrary.wiley.com/doi/abs/10.1002/joc.6967>.
- A. J. Matthews. Dynamical propagation and growth mechanisms for convectively coupled equatorial Kelvin waves over the Indian Ocean. Quarterly Journal of the Royal Meteorological Society, 147(741):4310–4336, 2021. doi: <https://doi.org/10.1002/qj.4179>. URL <https://rmets.onlinelibrary.wiley.com/doi/abs/10.1002/qj.4179>.
- M. B. Menary, T. Kuhlbrodt, J. Ridley, M. B. Andrews, O. B. Dimdore-Miles, J. Deshayes, R. Eade, L. Gray, S. Ineson, J. Mignot, C. D. Roberts, J. Robson, R. A. Wood, and P. Xavier. Preindustrial Control Simulations With HadGEM3-GC3.1 for CMIP6. Journal of Advances in Modeling Earth Systems, 10(12):3049–3075, 2018. doi: <https://doi.org/10.1029/2018MS001495>. URL <https://agupubs.onlinelibrary.wiley.com/doi/abs/10.1029/2018MS001495>.
- T. Nakazawa. Tropical Super Clusters within Intraseasonal Variations over the Western Pacific. Journal of the Meteorological Society of Japan. Ser. II, 66(6):823–839, 1988. doi: 10.2151/jmsj1965.66.6_823.
- S. C. Peatman, A. J. Matthews, and D. P. Stevens. Propagation of the Madden–Julian Oscillation through the Maritime Continent and scale interaction with the diurnal cycle of precipitation. Quarterly Journal of the Royal Meteorological Society, 140(680):814–825, 2014. doi: 10.1002/qj.2161.
- S. C. Peatman, J. Schwendike, C. E. Birch, J. H. Marsham, A. J. Matthews, and G.-Y. Yang. A Local-to-Large Scale View of Maritime Continent Rainfall: Control by ENSO, MJO, and Equatorial Waves. Journal of Climate, 34(22):8933 – 8953, 2021. doi: 10.1175/JCLI-D-21-0263.1. URL <https://journals.ametsoc.org/view/journals/clim/34/22/JCLI-D-21-0263.1.xml>.
- A. F. Prein, W. Langhans, G. Fosser, A. Ferrone, N. Ban, K. Goergen, M. Keller, M. Tölle, O. Gutjahr, F. Feser, E. Brisson, S. Kollet, J. Schmidli, N. P. M. van Lipzig, and R. Leung. A review on regional convection-permitting climate modeling: Demonstrations, prospects, and challenges. Reviews of Geophysics, 53(2):323–361, 2015. doi: <https://doi.org/10.1002/2014RG000475>. URL <https://agupubs.onlinelibrary.wiley.com/doi/abs/10.1002/2014RG000475>.
- A. Purwaningsih, S. W. Lubis, E. Hermawan, D. F. Andarini, T. Harjana, D. N. Ratri, A. Ridho, Risyanto, and A. P. Sujalu. Moisture Origin and Transport for Extreme Precipitation over Indonesia’s New Capital City, Nusantara in August 2021. Atmosphere, 13(9), 2022. ISSN 2073-4433. doi: 10.3390/atmos13091391. URL <https://www.mdpi.com/2073-4433/13/9/1391>.
- J.-H. Qian. Why Precipitation Is Mostly Concentrated over Islands in the Maritime Continent. Journal of the Atmospheric Sciences, 65(4):1428 – 1441, 2008. doi: 10.1175/2007JAS2422.1. URL <https://journals.ametsoc.org/view/journals/atsc/65/4/2007jas2422.1.xml>.

- C. S. Ramage. Role of a tropical "Maritime Continent" in the atmospheric circulation. *Monthly Weather Review*, 96(6):365 – 370, 1968. doi: 10.1175/1520-0493(1968)096<0365:ROATMC>2.0.CO;2. URL https://journals.ametsoc.org/view/journals/mwre/96/6/1520-0493_1968_096_0365_roatmc_2_0_co_2.xml.
- M. J. Roberts, A. Baker, E. W. Blockley, D. Calvert, A. Coward, H. T. Hewitt, L. C. Jackson, T. Kuhlbrodt, P. Mathiot, C. D. Roberts, R. Schiemann, J. Seddon, B. Vannière, and P. L. Vidale. Description of the resolution hierarchy of the global coupled HadGEM3-GC3.1 model as used in CMIP6 HighResMIP experiments. *Geoscientific Model Development*, 12(12): 4999–5028, 2019. doi: 10.5194/gmd-12-4999-2019. URL <https://gmd.copernicus.org/articles/12/4999/2019/>.
- P. E. Roundy. Analysis of Convectively Coupled Kelvin Waves in the Indian Ocean MJO. *Journal of the Atmospheric Sciences*, 65(4):1342 – 1359, 2008. doi: 10.1175/2007JAS2345.1. URL <https://journals.ametsoc.org/view/journals/atsc/65/4/2007jas2345.1.xml>.
- N. Sakaeda, G. Kiladis, and J. Dias. The Diurnal Cycle of Rainfall and the Convectively Coupled Equatorial Waves over the Maritime Continent. *Journal of Climate*, 33(8):3307 – 3331, 2020. doi: 10.1175/JCLI-D-19-0043.1. URL <https://journals.ametsoc.org/view/journals/clim/33/8/jcli-d-19-0043.1.xml>.
- E. Short, C. L. Vincent, and T. P. Lane. Diurnal Cycle of Surface Winds in the Maritime Continent Observed through Satellite Scatterometry. *Monthly Weather Review*, 147(6):2023 – 2044, 2019. doi: 10.1175/MWR-D-18-0433.1. URL <https://journals.ametsoc.org/view/journals/mwre/147/6/mwr-d-18-0433.1.xml>.
- K. H. Straub and G. N. Kiladis. The Observed Structure of Convectively Coupled Kelvin Waves: Comparison with Simple Models of Coupled Wave Instability. *Journal of the Atmospheric Sciences*, 60(14):1655 – 1668, 2003. doi: 10.1175/1520-0469(2003)060<1655:TOSOCC>2.0.CO;2. URL https://journals.ametsoc.org/view/journals/atsc/60/14/1520-0469_2003_060_1655_tosocc_2_0_co_2.xml.
- R. van der Linden, A. H. Fink, J. G. Pinto, T. Phan-Van, and G. N. Kiladis. Modulation of Daily Rainfall in Southern Vietnam by the Madden-Julian Oscillation and Convectively Coupled Equatorial Waves. *Journal of Climate*, 29(16):5801 – 5820, 2016. doi: 10.1175/JCLI-D-15-0911.1. URL <https://journals.ametsoc.org/view/journals/clim/29/16/jcli-d-15-0911.1.xml>.
- K. Van Weverberg, C. J. Morcrette, I. Boutle, K. Furtado, and P. R. Field. A Bimodal Diagnostic Cloud Fraction Parameterization. Part I: Motivating Analysis and Scheme Description. *Monthly Weather Review*, 149(3):841 – 857, 2021. doi: 10.1175/MWR-D-20-0224.1. URL <https://journals.ametsoc.org/view/journals/mwre/149/3/MWR-D-20-0224.1.xml>.
- C. L. Vincent, T. P. Lane, and M. C. Wheeler. A local index of Maritime Continent intraseasonal variability based on rain rates over the land and sea. *Geophysical Research Letters*, 43(17):9306–9314, 2016. doi: <https://doi.org/10.1002/2016GL069987>. URL <https://agupubs.onlinelibrary.wiley.com/doi/abs/10.1002/2016GL069987>.
- D. Walters, I. Boutle, M. Brooks, T. Melvin, R. Stratton, S. Vosper, H. Wells, K. Williams, N. Wood, T. Allen, A. Bushell, D. Copsey, P. Earnshaw, J. Edwards, M. Gross, S. Hardiman, C. Harris, J. Heming, N. Klingaman, R. Levine, J. Manners, G. Martin, S. Milton, M. Mittermaier, C. Morcrette, T. Riddick, M. Roberts, C. Sanchez, P. Selwood, A. Stirling, C. Smith, D. Suri, W. Tennant, P. L. Vidale, J. Wilkinson, M. Willett, S. Woolnough, and P. Xavier. The Met Office Unified Model Global Atmosphere 6.0/6.1 and JULES Global Land 6.0/6.1 configurations. *Geoscientific Model Development*, 10(4):1487–1520, 2017. doi: 10.5194/gmd-10-1487-2017. URL <https://gmd.copernicus.org/articles/10/1487/2017/>.
- M. Wheeler and G. N. Kiladis. Convectively Coupled Equatorial Waves: Analysis of Clouds and Temperature in the Wavenumber-Frequency Domain. *Journal of the Atmospheric Sciences*, 56(3):374 – 399, 1999. doi: 10.1175/1520-0469(1999)056<0374:CCEWAO>2.0.CO;2. URL https://journals.ametsoc.org/view/journals/atsc/56/3/1520-0469_1999_056_0374_ccewao_2_0_co_2.xml.
- K. D. Williams, D. Copsey, E. W. Blockley, A. Bodas-Salcedo, D. Calvert, R. Comer, P. Davis, T. Graham, H. T. Hewitt, R. Hill, P. Hyder, S. Ineson, T. C. Johns, A. B. Keen, R. W. Lee, A. Megann, S. F. Milton, J. G. L. Rae, M. J. Roberts, A. A. Scaife, R. Schiemann, D. Storkey, L. Thorpe, I. G. Watterson, D. N. Walters, A. West, R. A. Wood, T. Woollings, and P. K. Xavier. The Met Office Global Coupled Model 3.0 and 3.1 (GC3.0 and GC3.1) Configurations. *Journal of Advances in Modeling Earth Systems*, 10(2):357–380, 2018. doi: <https://doi.org/10.1002/2017MS001115>. URL <https://agupubs.onlinelibrary.wiley.com/doi/abs/10.1002/2017MS001115>.

- D. R. Wilson and S. P. Ballard. A microphysically based precipitation scheme for the UK meteorological office unified model. *Quarterly Journal of the Royal Meteorological Society*, 125(557):1607–1636, 1999. doi: <https://doi.org/10.1002/qj.49712555707>. URL <https://rmets.onlinelibrary.wiley.com/doi/abs/10.1002/qj.49712555707>.
- D. R. Wilson, A. C. Bushell, A. M. Kerr-Munslow, J. D. Price, and C. J. Morcrette. PC2: A prognostic cloud fraction and condensation scheme. I: Scheme description. *Quarterly Journal of the Royal Meteorological Society*, 134(637):2093–2107, 2008. doi: <https://doi.org/10.1002/qj.333>. URL <https://rmets.onlinelibrary.wiley.com/doi/abs/10.1002/qj.333>.
- P. Wu, M. Hara, J-i Hamada, M. D. Yamanaka, and F. Kimura. Why a Large Amount of Rain Falls over the Sea in the Vicinity of Western Sumatra Island during Nighttime. *Journal of Applied Meteorology and Climatology*, 48(7):1345 – 1361, 2009. doi: 10.1175/2009JAMC2052.1. URL <https://journals.ametsoc.org/view/journals/apme/48/7/2009jamc2052.1.xml>.
- G.-Y. Yang and Julia Slingo. The Diurnal Cycle in the Tropics. *Monthly Weather Review*, 129(4):784 – 801, 2001. doi: 10.1175/1520-0493(2001)129<0784:TDCITT>2.0.CO;2. URL https://journals.ametsoc.org/view/journals/mwre/129/4/1520-0493_2001_129_0784_tdcitt_2.0.co_2.xml.